Electronic supplementary information for:

Exploiting the versatile alkyne-based chemistry for expanding the applications of a stable triphenylmethyl organic radical on surfaces

J. Alejandro de Sousa, Francesc Bejarano, Diego Gutiérrez, Yann R. Leroux, Ewa-Malgorzata Nowik Boltyk, Tobias Junghoefer, Erika Giangrisostomi, Ruslan Ovsyannikov, Maria Benedetta Casu, Jaume Veciana, Marta Mas-Torrent, Bruno Fabre, Concepció Rovira, Núria Crivillers

Table of contents

1-Materials

All reagents used were of high quality. Ferrocenemethanol, glacial acetic acid, copper (I) iodide, aqueous 54-56% tetrabutylammonium hydroxide, tetrabutylammonium hexafluorophosphate 98% and *N*,*N*-diisopropylethylamine (DIPEA) were obtained from Sigma-Aldrich. Sodium azide and *p*-chloranil were obtained from Panreac.

All solvents were of HPLC grade. Toluene and THF were dried using sodium and benzophenone as indicator before use; acetonitrile and dichloromethane were dried using CaH_2 before use. The purification of the synthesised compounds was carried out using Carlo Erba silica gel (60, particle size 35-70).

2-Apparatus

2.1-Electrochemical measurements.

2.1.1-Silicon Surface

Cyclic voltammetry measurements were performed with an Autolab electrochemical analyzer (PGSTAT 30 potentiostat/galvanostat from Eco Chemie B.V.) equipped with the GPES and FRA softwares in a home-made three-electrode glass cell. The working electrode, modified Si(111), was pressed against an opening in the cell side using a Teflon circular piece and a FETFE (Aldrich) O-ring seal. An ohmic contact was made on the previously polished rear side of the sample by applying a drop of In-Ga eutectic (Alfa-Aesar, 99.99%). A steel piece was dropped on the eutectic-coated sample and then the assembly was screwed to the cell using a plastic cap screw. The electrochemically active area of the Si(111) surface (namely 0.3 cm^2) was estimated by measuring the charge under the voltammetric peak corresponding to the ferrocene oxidation on Si(111)-H and compared to that obtained with a 1 cm^2-Pt electrode under the same conditions. The counter electrode was a carbon rod and the system 10^{-2} M Ag^+ | Ag in acetonitrile was used as the reference electrode (+0.33 V versus aqueous Ag/AgCl, KCl 3M). All reported potentials are referred to Ag/AgCl, KCl 3M (uncertainty ± 5 mV). Tetra-n-butylammonium perchlorate Bu_4NClO_4 (Fluka, puriss, electrochemical grade) was used at 0.1 mol L^{-1} as supporting electrolyte in acetonitrile. The (CH_3CN + 0.1 M Bu_4NClO_4) electrolytic medium was dried over activated, neutral alumina (Merck) for 30 min, under stirring and under argon. About 20 mL of this solution was transferred with a syringe into the electrochemical cell prior to experiments. All electrochemical measurements were carried out inside a home-made Faraday cage, at room temperature (20 ± 2 ºC) under constant argon gas flow. The light was provided by a solar simulator with a fluence of 100 mW cm^{-2}

(LS0106, LOT Quantum Design) equipped with a AM 1.5G and red (Edmund Optics) filters. For impedance spectroscopy measurements, the amplitude of the alternating current (ac) signal was 10 mV. The differential capacitance C was determined from the imaginary part (Z") of the complex impedance Z″ ($C = -1/2\pi fZ''$) where f is the frequency. For Mott-Schottky experiments, the cell was in the dark and the potential was swept from positive to negative values at a frequency of 50 kHz (25 mV step potential).

2.1.2-Gold Surface

Cyclic voltammetry, square wave voltammetry and impedance spectroscopy characterizations were performed with an AUTOLAB 204 equipped with NOVA 2.3 software. A Pt mesh was used as the counter electrode, Ag/AgCl 3M KCl was used as reference electrode. Studies in solution were made using a glassy carbon as the working electrode (Area = 0.28 cm^2). For the electrochemical characterization of the SAMs, the modified Au^{TS} was used as the working electrode (area exposed of 1 cm^2). A 0.1M or 0.2M solution of $TBAPF_6$ in dry CH_2Cl_2 was used as the electrolytic medium, under argon atmosphere.

For impedance measurements, the frequency was scanned from 100 kHz to 0.1 Hz with a 20 mV amplitude. Four different potentials were applied: -0.5, 0, 0.3 and 0.7 V vs Ag/AgCl 3M KCl.

2.2-Electron Paramagnetic Resonance (EPR) spectroscopy.

EPR spectra were recorded at room temperature on a Bruker ESP 300 E spectrometer provided with a rectangular cavity T102 that works with an X band (9.5 GHz). The signal-to-noise ratio of spectra was increased by accumulation of scans using the F/Flock accessory to guarantee large field reproducibility. Precautions to avoid undesirable spectral distortion and line broadenings, such as those arising from microwave power saturation and magnetic field over modulation, were also taken into account to improve sensitivity.

2.3-UV-vis absorption spectroscopy.

UV-Vis spectra were obtained from a Varian Cary 5000 UV-Vis-NIR spectrophotometer. Quartz cuvettes with an optical path of 1 cm were used in all experiments.

2.4-MALDI-ToF mass spectroscopy.

The reported spectra were acquired with a Bruker Ultraflex mass spectrometer by operating at ion pulsed extraction in negative mode at high power. Ditranol was used as a matrix to improve the laser absorption.

2.5-Nuclear magnetic resonance spectroscopy (NMR).

The ^{1}H-NMR spectra were acquired with a Bruker Avance DPX (250 MHz) spectrometer and Bruker Avance-II+ (600MHz)), ^{13}C-NMR spectra were obtained from a Bruker Avance-III (400MHz) spectrometer. The calibration was made using residual nondeuterated chloroform (δ(1H) = 7.26 ppm; δ(13C) = 77.00 ppm) as internal references. The data analysis was carried out with MestReNova software (MestReLab Research S. L.). The following abbreviations were used to designate multiplicities: s = singlet, d = doublet, m = multiplet.

2.6-Infrared spectroscopy (IR).

The spectra were obtained from a FT-IR PerkinElmer spectrometer with a diamond ATR accessory.

2.7-X-ray photoelectron spectroscopy (XPS).

2.7.1-Silicon surface characterization.

XPS measurements were performed with an Mg K_{alpha} ($h\upsilon$ = 1254.6 eV) X-ray source and an Al source ($h\upsilon$= 1486.6 eV) using a VSW HA100 photoelectron spectrometer with a hemispherical photoelectron analyzer, working at an energy pass of 20 eV for survey and resolved spectra. The experimental resolution was 1.0 eV. Unless specified, C1s set at 285.0 eV was used as the energy reference for all the analyses.

2.7.2-Gold surface characterization.

X-ray Photoelectron Spectroscopy (XPS) measurements were performed in an analysis chamber (base pressure 2 x 10^{-10} mbar) equipped with a monochromatic Al Kα source (SPECS XR 50 M plus SPECS Focus 500) and a SPECS Phoibos 150 hemispherical electron analyser. The detailed spectra were measured at 20 eV pass energy, the survey spectra at 50 eV pass energy, and their binding energy calibrated to the Au 4f signal at 84 eV. NEXAFS and photon dependent XPS measurements were performed at the third-generation synchrotron radiation source Bessy II (Berlin) at the LowDose PES end-station, at the PM4 beamline, equipped with a Scienta ArTOF-10k spectrometer. The measurements were carried out in multibunch hybrid mode (ring current in top up mode = 250 mA, cff = 1.6, 100-μm exit slit, estimated energy resolution = 340 meV at 640 eV). The NEXAFS spectra, measured in total electron yield, were normalized by using the clean substrate signal and the ring current into account, and then all spectra were scaled to give an equal edge jump.[1–3] No beam-induced degradation of the samples was observed on the time scale of all discussed experiments.

2.8-Transport measurements through Au^{TS}/SAM//GaOx/EGaIn junctions.

The "EGaIn measurements" were performed using a home-made measurement set-up. The *J-V* curves were acquired using a Keithley 2004B. The Keithley was controlled using in-house software developed with LabVIEW. During the measurements, the top-electrode GaOx/EGaIn was biased and the bottom electrode was grounded.

3. Synthesis and characterization of the synthesised compounds.

3.1-Synthesis of azidomethylferrocene.

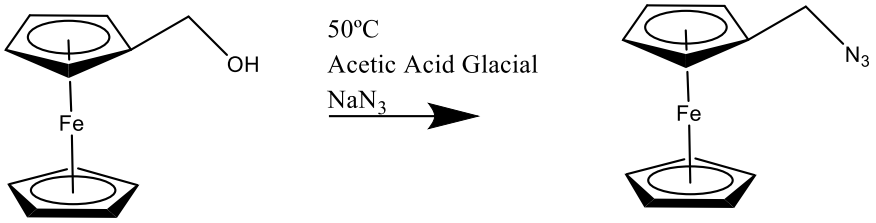

Scheme S 1. Synthesis of azidomethylferrocene.

Azidomethylferrocene was synthesized using the procedure reported by J.M. Casas-Solvas[4]. Ferrocenemethanol (133.0 mg, 0.6 mmol) and sodium azide (239.7 mg, 0.99 mmol) were mixed in glacial acetic acid (3 mL) and stirred at 50 ºC for 2 h. The resulting mixture was diluted in CH_2Cl_2 (50 mL) and the organic phase was washed with a saturated solution of $NaHCO_3$ (3 x 50 mL), dried (Mg_2SO_4), filtered and evaporated under vacuum. After column chromatography (silica gel, EtOAc:Hexane, 1:25) the desired compound was obtained as an orange oil (139 mg, 96%). **^{1}H-NMR** ($CDCl_3$, 250 MHz): δ(ppm)= 4.12 (s, 2H, **CH_2**); δ= 4.17 (s, 5H, Cp-**H**); δ= 4.20 (t, 2H, Cp-**H**); δ= 4.23 (t, 2H, Cp-**H**). ATR-IR: ν (cm^{-1}) = 3092 (Cp-H), 2923 (C-H), 2856(C-H), 2088 (ν_{as} $N=N^+-N^-$),1252 (ν_{as} $N=N^+-N^-$).

3.2-Synthesis of PTM-Fc alpha H compounds: 3-H and 4-H.

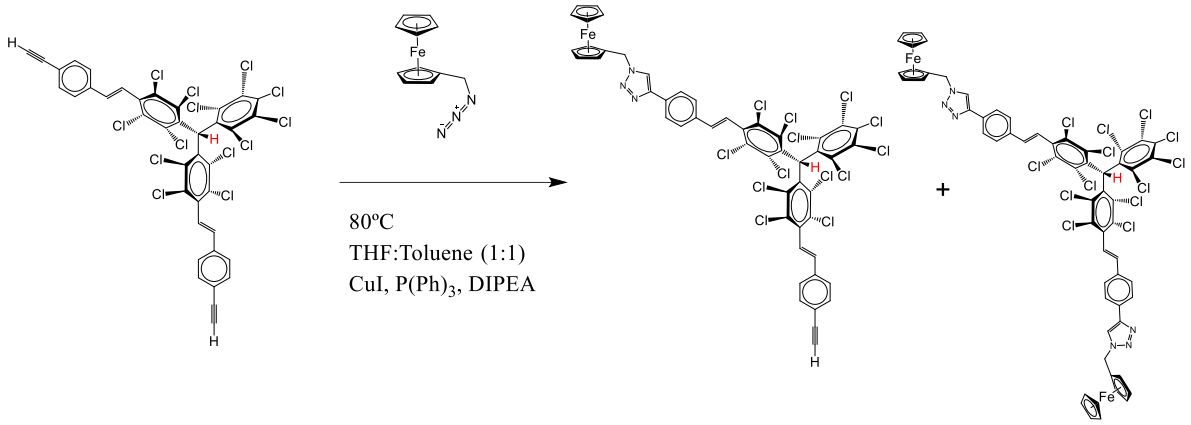

2-H 3-H 4-H

Scheme S2. Synthesis of compounds **3-H** and **4-H**.

Azidomethylferrocene (12.6 mg, 0.052 mmol) dissolved in 1 mL of dry THF was added to a mixture of diacetylene derivative **2-H** (50.4 mg, 0.053mmol) triphenylphosphine (8.1 mg, 0.031 mmol), CuI (6.4 mg, 0.0336 mmol) and *N*,*N*-diisopropylethylamine (DIPEA, 10.61 M; 50 μL, 0.265 mmol) in 1 mL of dry toluene. The mixture was stirred for 3 hours at 80°C under argon atmosphere. The resulting mixture was evaporated and the obtained solid dissolved in 20 mL of toluene. To remove the unreacted CuI, the resulting solution was vigorously washed (3 x 50mL) with a solution of 0.5 M of EDTA and 0.2M of NH_3 (the pH of the solution was adjusted to 9 with NaOH). This rinsing process consisted in stirring the organic phase for 3 hours with the washing aqueous solution. This was repeated three times. Finally, the organic phase was dried (Na_2SO_4), filtered and evaporated under vacuum. After evaporation of the solvent, the crude was purified by column chromatography with silica gel using as eluent CH_2Cl_2 to get pure αH-PTM-Fc (**3-H**) and then a gradient with $CHCl_3$ to have the αH-PTM-Fc2 (**4-H**). Both mono- and di- cycloaddition products were obtained as a yellow powder with a yield of 38 % (**3-H**) and 35% (**4-H**).

αH-PTM-Fc (3-H): ^{1}**H NMR** ($CDCl_3$, 600 MHz): δ(ppm) = 7.83 (d, 2H, *J*=8.18 Hz, Ar-**H**), 7.67 (s, 1H, N-**H**), 7.57 (d, 2H, *J*=8.21 Hz, Ar-**H**), 7.52 (d, 2H, *J*=8.21 Hz, Ar-**H**), 7.50 (d, 2H, *J*=8.26 Hz, Ar-**H**), 7.08-7.07 (m, 5H, **H**-C=C-**H and α H**), 5.36 (s, 2H, **CH_2**), 4.33 (m, 2H, **C_9-H**), 4.25 (m, 2H, **C_8-H**), 4.21 (s, 5H, **C_{10}-H**), 3.16 (s, 1H, C≡C-**H**); ^{13}**C NMR** ($CDCl_3$, 101 MHz): δ =147.17 (**C-1**), 137.98, 137.58, 137.33, 136.99, 136.70, 136.45, 136.40, 135.73, 135.22, 135.18, 135.05, 134.96, 134.91, 134.04, 133.98, 133.49, 133.40, 132.62, 132.44, 132.26, 131.21, 128.59, 127.99, 127.44, 126.84, 126.06, 125.68, 124.19, 123.16, 122.51, 119.12

(**C-2**), 83.47 (**C≡C-H**), 80.74 (**C-7**), 78.55 (**C≡C-H**), 69.22 (**C-9**), 69.05 (**C-8**), 69.02 (**C-10**), 56.83 **(αH-C)**, 50.27 (**C-6**).

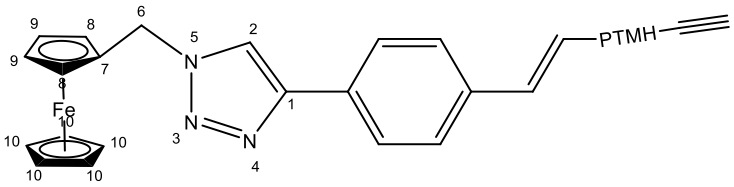

ATR-IR: ν (cm^{-1}) = 3298 (w) (CΞC-H), 3082 (w) (ArC-H), 3032 (w) (C=C-H), 2106 (w) (CΞC), 1632 (w) (C=C), 1611 (w), 1537 (w) (ArC-ArC), 1504 (w) (ArC-ArC),1454 (w) (N=N), 1413 (w) (Cl-ArC-ArC-Cl), 1360 (m) (Cl-ArC-ArC-Cl), 1334 (m) (Cl-ArC-ArC-Cl), 1291 (s), 1263 (m), 1230 (w), 1180 (w), 1138 (w), 1106 (w), 1041 (w) (C-N), 969 (w), 806 (ArC-Cl). **LDI-ToF** *m/z* $[M]^-$ calcd for $C_{50}H_{26}Cl_{13}FeN_3$, 1184.73; found, *1184.18* $[M-H]^+$; **UV/Vis (CH_2Cl_2):** λ (nm) (ε) 317.54 (60091), 434.36 (113). **CV** (0.1 M $TBAPF_6$ in CH_2Cl_2, vs Ag/AgCl KCl 3M): $E_{1/2}(Fc^+/Fc)$ = 0.60V

αH-PTM-Fc2 (4-H). ^{1}H NMR (CD_2Cl_2, 600 MHz): δ(ppm) = 7.83 (d, 4H, *J*=8.17 Hz, Ar-**H**), 7.67 (s, 1H, N-**H**), 7.57 (d, 4H, *J*=8.21 Hz, Ar-**H**), 7.08 (bs, 4H, **H**-C=C-**H**), 7.07 (s, 1H, **α H**), 5.36 (s, 4H, **CH_2**), 4.33 (m, 4H, **C_{p9}-H**), 4.25 (m, 4H, **C_{p8}-H**), 4.21 (s, 10H, **C_{p10}-H**); **^{13}C NMR ($CDCl_3$, 101 MHz):** δ(ppm)=147.16 (**C-1**), 137.95, 137.29, 137.27, 137.03, 136.45, 136.42, 135.73, 135.20, 134.99, 134.89, 134.05, 133.98, 133.96, 133.46, 133.40, 133.35, 132.40, 132.26, 132.22, 131.18, 127.43, 126.05, 123.17, 119.15 (**C-2**), 80.79 (**C-7**), 69.29 (**C-9**), 69.12 (**C-8**), 69.09 (**C-10**), 56.82 (**αH-C)**, 50.29 (**C-6**).

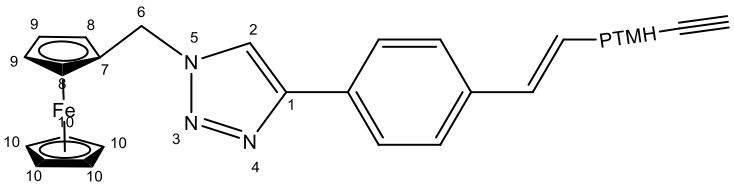

ATR-IR: ν (cm^{-1}) = 3090 (w) (ArC-H), 3037 (w) (C=C-H), 1632 (w) (C=C), 1610 (w) , 1537(w) (ArC-ArC), 1504 (w) (ArC-ArC), 1453 (w) (N=N), 1411 (w) (Cl-ArC-ArC-Cl), 1364 (m) (Cl-ArC-ArC-Cl), 1329 (m) (Cl-ArC-ArC-Cl), 1298 (s), 1272 (m), 1179 (w), 1141 (w), 1105 (w), 1068 (w), 1041 (w) (C-N), 966 (w), 806 (ArC-Cl); **LDI-ToF** (negative mode): *m/z* calcd. for $C_{61}H_{37}Cl_{13}Fe_2N_6$, 1425.76; found, 1425.21$[M]^+$; **UV/Vis (CH_2Cl_2):** λ (nm) (ε) 325.46 (76303), 432.38 (291). **CV** (0.1 M $TBAPF_6$ in CH_2Cl_2, vs Ag/AgCl KCl 3M): $E_{1/2}(Fc^+/Fc)$ = 0.61V.

3.3-Synthesis of PTM-Fc radicals compounds 3-Rad and 4-Rad

Two different synthetic routes (A and B) were followed to obtain **3-Rad** and **4-Rad**

Route A:

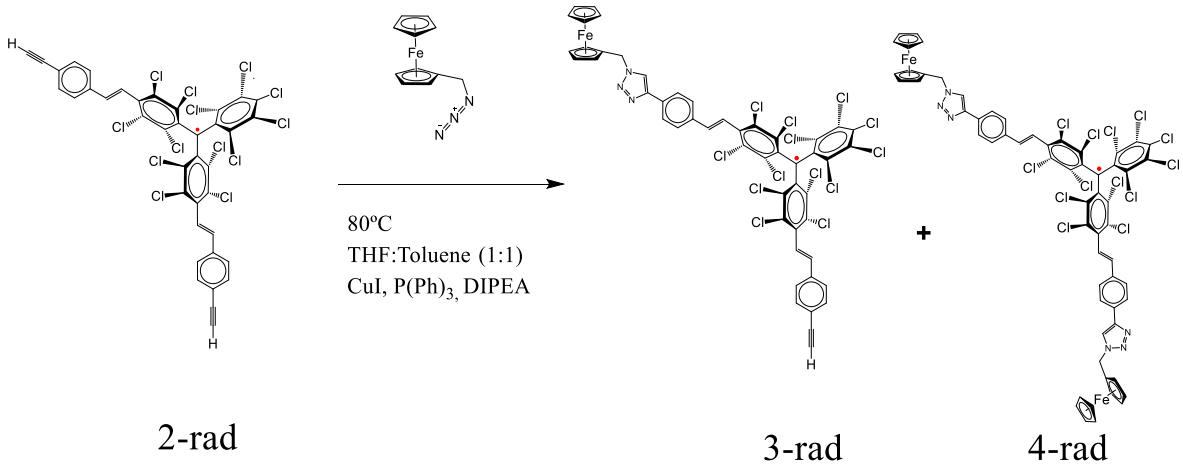

Scheme S3. Synthesis of compounds **3-Rad** and **4-Rad** by route A.

Route A: All the process was carried out in a laboratory equipped with red light to avoid the decomposition of the radical species in solution. Azidomethylferrocene (12.4 mg, 0.0515 mmol) dissolved in 1 mL of dry THF was added to a mixture of diacetylene derivative **2-Rad** (50.1 mg, 0.0530 mmol) triphenylphosphine (8 mg, 0.0305 mmol), CuI (6 mg, 0.0315 mmol) and *N*,*N*-diisopropylethylamine (DIPEA, 10.61 M; 50 μL, 0.26525 mmol) in 1 mL of dry toluene. The mixture was stirred for 3 hours at 80°C under argon atmosphere. The resulting mixture was evaporated and the obtained solid dissolved in 20 mL of toluene. To remove the unreacted CuI, the resulting solution was vigorously washed (3 x 50mL) with a solution of 0.5 M of EDTA and 0.2M of NH_3 (the pH of the solution was adjusted to 9 with NaOH). This rinsing process consisted in stirring the organic phase for 3 hours with the washing aqueous solution. This was repeated three times. Finally, the organic phase was dried (Na_2SO_4), filtered and evaporated under vacuum. After evaporation of the solvent, the crude was purified by column chromatography with silica gel using as eluent CH_2Cl_2 to the rad-PTM-Fc (**3-Rad**) and then a gradient with $CHCl_3$ to have the rad-PTM-Fc2 (**4-Rad**). Both mono- and di-cycloaddition products were obtained as a dark brown powder with a yield of 51% (**3-Rad**) and 48% (**4-Rad**).

Route B:

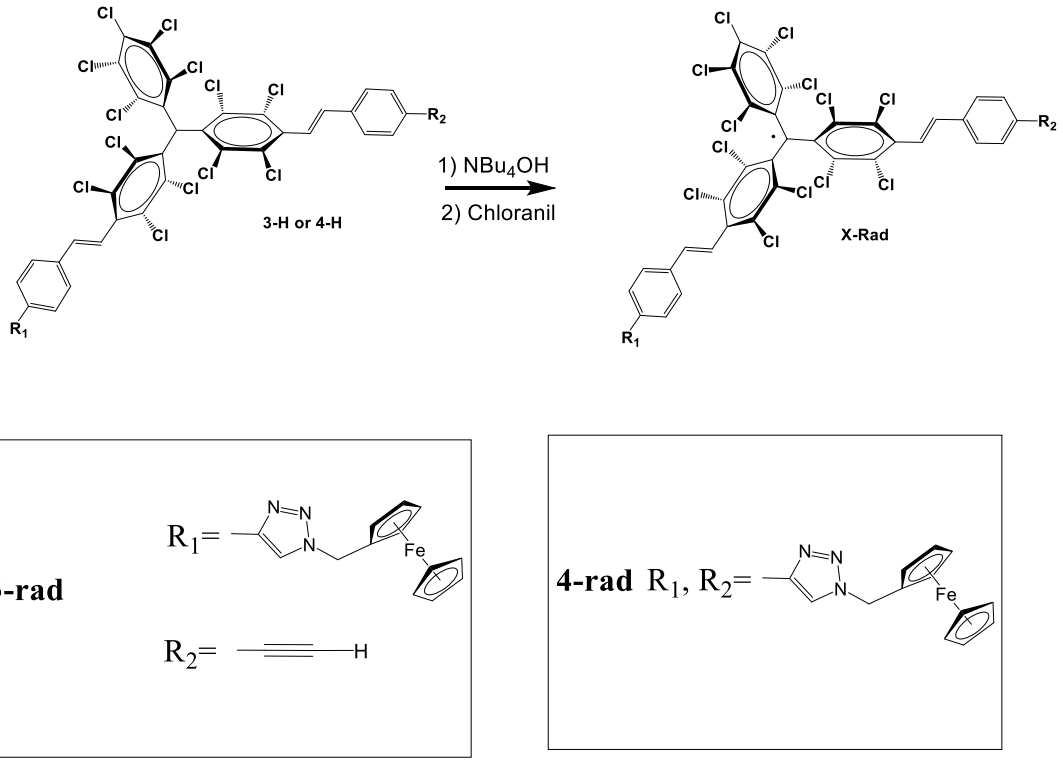

Scheme S4. Synthesis of compounds **3-Rad** and **4-Rad** by route B.

Route B

Synthesis of compound 3-Rad. All the process was carried out in a laboratory equipped with red light to avoid the decomposition of the radical species in solution. Tetrabutyl ammonium hydroxide 28 % aqueous (14 μL, 0.0151 mmol) was added to a solution of compound **3-H** (14.9 mg, 0.0126 mmol) in dry THF (5 mL) and the solution was stirred at room temperature. The formation of the perchlorotriphenylmethyl anion was monitored by UV/vis spectroscopy. When the deprotonation is complete (about 30 min), *p*-chloranil was added (3.9 mg, 0.0158 mmol) and the oxidation from the perchlorotriphenylmethyl anion to the radical was followed by UV/vis spectroscopy. When the oxidation was complete (about 180 min) the mixture was evaporated under vacuum and the crude was purified by column chromatography (silica gel, CH_2Cl_2). Compound **3-Rad** was obtained as a dark brown powder (13.5 mg, 90% yield).

ATR-IR: ν (cm^{-1}) = 3294 (w) (C≡C-H), 3078 (w) (ArC-H), 3032 (w) (ArC-H),2926 (w), 2854 (w), 2106 (w) (C≡C), 1681 (w) (C=C), 1609 (w), 1506 (w) (ArC-ArC), 1336 (m) (Cl-ArC-ArC-Cl), 1321 (m) (Cl-ArC-ArC-Cl), 1292 (w) (Cl-ArC-ArC-Cl), 1259 (w) (Cl-ArC-ArC-Cl), 1208 (w) (Cl-ArC-ArC-Cl), 1041 (m) (C-N), 970 (m), 817 (s) (C-Cl), **LDI-ToF** (negative mode) m/z: $[M]^-$ calcd for $C_{50}H_{25}Cl_{13}FeN_3$, 1183.73; found, 1183.18, **UV/Vis** (CH_2Cl_2): λ (nm) (ε)

308.96 (37809), 380.96 (17797), 442.28 (18400), 586.82 (2299); **CV** (0.1 M $TBAPF_6$ in CH_2Cl_2, vs Ag/AgCl KCl 3M): $E_{1/2}$(radical/anion) = -0.17V, $E_{1/2}(Fc^+/Fc)$ = 0.61; **EPR**: g = 2.0026, $a(^1H)$ = 1.9 G, ΔH_{pp} = 1.1 G, $a(^{13}CAr)$ = 12.6, 14.3 G, $a(^{13}C\alpha)$ = 29.4 G.

Synthesis of compound 4-Rad: Compound **4-H** (40.3 mg, 0.0282 mmol) was dissolved in dry THF (5 mL). 56 % aqueous tetrabutyl ammonium hydroxide (16 μL, 0.0339 mmol) was added and the solution was stirred at room temperature. The formation of the perchlorotriphenylmethyl anion was monitored by UV/vis spectroscopy. When the deprotonation is complete (about 20 min) *p*-chloranil (9.4 mg, 0.0382 mmol) was added and the oxidation to the radical was followed by UV/vis spectroscopy. When the oxidation was complete (about 180 min) the mixture was evaporated under vacuum and the crude was purified by column chromatography (silica gel, chloroform). Compound **4-Rad** was obtained as a dark brown powder (39.5 mg, 98% yield).

ATR-IR: ν (cm^{-1}) = 3139 (w) (ArC-H), 3085 (w) (ArC-H), 2924 (w), 2852 (w), 1625 (w) (C=C), 1497 (w) (ArC-ArC), 1325 (m) (Cl-ArC-ArC-Cl), 1294 (w) (Cl-ArC-ArC-Cl), 1258 (w) (Cl-ArC-ArC-Cl), 1224 (w) (Cl-ArC-ArC-Cl), 1177 (w), 1105 (w), 1040 (m) (C-N), 1000 (m), 817 (s) (C-Cl), **LDI-ToF** (negative mode): m/z calcd for $C_{61}H_{36}Cl_{13}Fe_2N_6$, 1424.76; found, 1424.07 $[M]^-$; **UV/Vis** (CH_2Cl_2): λ (nm) (ε) 316.22 (44431), 379.58 (24347), 448.88 (20665), 605.96 (2277); **CV** (0.1 M $TBAPF_6$ in CH_2Cl_2, vs Ag/AgCl KCl 3M): $E_{1/2}$(radical/anion) = -0.21V, $E_{1/2}(Fc^+/Fc)$ = 0.60; **EPR**: g = 2.0026, $a(^1H)$ = 1.9 G, ΔH_{pp} = 1.1 G, $a(^{13}CAr)$ = 12.6, 14.3 G, $a(^{13}C\alpha)$ = 29.4 G

4-General Procedures.

4.1- Templated stripped gold (Au^{TS}) substrates preparation.

Ultra-smooth template-striped gold substrates were prepared following a reported procedure[5] by thermal deposition of 200 nm of gold (99.999% purity) on a silicon (100) wafer with a native SiO_2 surface layer; the deposition parameters were 4 x 10^{-7} mTorr and rate 2A/s. After deposition, glass slides (1.5 cm^2) were glued onto the exposed gold using an epoxy resin (EpoTek, 353ND), the adhesive was cured at 80 °C for 12 hours in an oven. The glass/epoxy/metal substrate was cleaved from the Si wafer just before immersion into the desired solution, in order to minimize the contamination from air, and without any further cleaning procedure.

4.2-SAMs preparation.

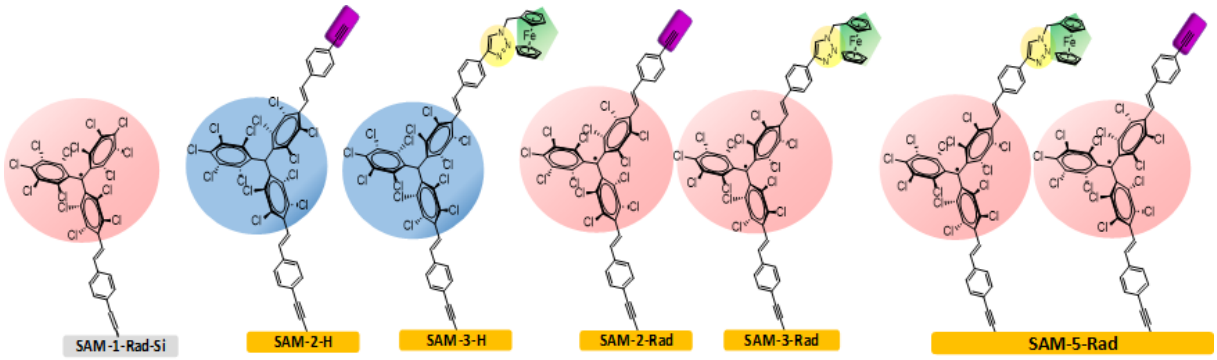

Scheme S5. SAMs prepared in this work.

4.2.1-Preparation of PTM radical-Modified Si(111) Surfaces (SAM-1-Rad-Si).

The chemicals used for cleaning and etching silicon wafer pieces (30% H_2O_2, 96-97% H_2SO_4 and 40% NH_4F solutions) were of VLSI semiconductor grade (Riedel-de-Haën). All Teflon vials used for cleaning of silicon were previously decontaminated in 3:1 v/v concentrated H_2SO_4/30% H_2O_2 at 100°C for 30 min, followed by copious rinsing with ultra-pure water.

***Caution**: The concentrated H_2SO_4:H_2O_2 (aq) piranha solution is very dangerous, particularly in contact with organic materials, and should be handled extremely carefully.*

All single side polished Si(111) samples (*p*-type, boron doped, 1-10 Ω cm, thickness = 525±25 μm, from Siltronix) were cut into 1.5 × ~4.0 cm^2 pieces from the same silicon wafer to ensure the maximum reproducibility of hydrogen-terminated and further molecular monolayer-modified surfaces. The sample was sonicated for 10 min successively in acetone (MOS semiconductor grade, Carlo Erba), ethanol (99.8%, VLSI semiconductor grade) and ultra-pure 18.2 MΩ cm water (Elga Purelab Classic UV, Veolia). It was then cleaned in 3:1 v/v concentrated H_2SO_4/30% H_2O_2 at 100°C for 30 min, followed by copious rinsing with ultra-pure water. The surface was etched with argon-degassed ppb grade 40% aqueous NH_4F for 20 min at room temperature[6]. The NH_4F solution was thoroughly degassed with argon for at least 30 min prior to the immersion of the piranha-treated surface. After etching, the Si-H sample was rinsed with argon-saturated water, blown dry with argon, and transferred immediately into a Pyrex Schlenk tube containing deoxygenated **1-Rad** dissolved in an aromatic solvent. An aluminum foil was put around the glassware to avoid the possible photochemical degradation of

the PTM radical. The hydrosilylation reaction was thermally activated and the alkyne solution was kept under a pressure of argon during the reaction.
The grafting conditions were optimized in order to produce the PTM radical-terminated monolayers with the highest PTM surface coverage and the lowest oxidation level of the underlying silicon surface. Toluene (99.8% from Sigma-Aldrich), mesitylene (99% extra-pure from Acros, passed through an activated neutral alumina column, then distilled over sodium) and 1,2-dichlorobenzene (DCB, 98% extra dry, from Acros) were tested as solvents since it has been demonstrated that the use of aromatic solvents with high boiling point was an efficient method for producing high-quality and well-ordered organic monolayers on silicon[7]. Moreover, different temperatures and concentrations of **1-Rad** were also tested. (Table S1). The optimal reaction conditions yielding the highest surface coverage of the PTM radical were as follows: 145°C for 20 h using DCB as the solvent and a **1-Rad** concentration higher than 7 mM. After reaction, the **SAM-1-Rad-Si** surface was thoroughly rinsed with toluene and dichloromethane, then dried under argon.

Table S1. Different experimental conditions used for the optimization of the thermal grafting of **1-Rad** on Si-H. The optimal conditions are highlighted in green.

Entry	**1-Rad** concentration / mM	Solvent	Temperature /°C	Time / h	Surface coverage of PTM radical / mol cm^{-2} [a]
1	2	Toluene	90	20	5×10^{-12}
2	2	Mesitylene	155	3	No grafting[b]
3	2.3	Mesitylene	115	20	No grafting[b]
4	2.3	DCB	130	20	7×10^{-12}
5	7	DCB	145	20	8.5×10^{-11}

[a] Determined electrochemically from the integration of the anodic voltammetric peak observed for illuminated **SAM-1-Rad-Si**. [b] Under these conditions, the radical is not stable and the solution changed colour over time.

4.2.2-Preparation of PTM Radical-Modified Gold Surfaces.

To form the SAMs, the freshly cleaved Au^{TS} substrates were introduced into a flat bottom flask containing a toluene (freshly distilled) solution containing 0.5 mM

of the desired compound and the flask was closed, filled with argon and sealed. The solution was heated for 6 hours at 40ºC and left 42 h at room temperature in dark. Then, the substrates were removed from the flask, thoroughly rinsed with toluene, dried with nitrogen stream. Compounds **2-H**, **3-H**, **2-Rad** and **3-Rad** were used to form **SAM-2-H**, **SAM-3-H**, **SAM-2-Rad** and **SAM-3-Rad**, respectively.

4.3-Click reaction on gold surface.

Two different methods were tested:

Methods 1 and 2:

To obtain the catalyst solution, two separated solutions were prepared: **solution 1** was prepared by 3 min sonication of CuI (10.1 mg) in 2 mL of dry acetonitrile and, **solution 2** consisted of $P(Ph)_3$ (16.4 mg) and 50 μL of *N*,*N*-diisopropylethylamine (10.61 M) in 2 mL of dry toluene.

In a flat bottom flask, **solution 1** (200 μL) and **solution 2** (200 μL) were added to a 2 mM solution of the azidomethylferrocene in 5 mL of dry toluene (**Method 1**) or 5 mL of dry acetonitrile (**Method 2**) and then **SAM-2-Rad** was introduced and the flask sealed. The flask was heated for 8 hours at 60ºC under argon atmosphere and dark and then left for 1 hour to cool down to room temperature. After removing the substrates from the flask, they were thoroughly rinsed with a solution of 0.5 M of EDTA and 0.2M of NH_3, acetonitrile, toluene, acetone and dichloromethane and finally dried under nitrogen stream.

The yield of the reaction was estimated from the cyclic voltammetry experiments (see Figures S4-S8) leading to an approximate yield of 30% and 50% for **Methods 1** and **2**, respectively.

4.4-Surface Coverage Calculation.

The surface coverage was calculated from the Equation S1[8,9]:

$$\Gamma = \frac{A_{peak}}{nFSv} \qquad \text{Equation S1}$$

where Γ is the surface coverage in mol cm^{-2}, A_{peak} is the integrated area of the anodic or cathodic voltammetry peak, *n* is the number of electrons transferred (in this case n = 1), *F* is Faraday's constant, *S* is the electrode surface area and *v* is the scan rate.

4.5-Charge transport measurements through the SAMs on gold.

The modified Au^{TS} substrates were top-contacted with the GaOx/EGaIn tips. These tips were prepared following the F.C. Simeone[10] procedure. After the formation of the tip, this was gently approached to a clean silicon surface (50 nm SiO_2 polished) that helped to flatten the irregularities and roughness generated during the tip preparation.

The GaOx/EGaIn tip area used to contact the samples surfaces was around 1000-2500 μm^2 as it is recommended to obtain stable measurements [11].The top-electrode was biased and the bottom electrode was grounded. The top electrode was biased from 0V →1 V→ 0V → -1 V→ 0V. For each sample, 12 traces on 24 junctions were collected, with a step size of 50 mV, integration time of 100 ms, and a delay of 50 ms, for acquiring the *J*(*V*) curves. The tip was renewed every three junctions. Below, a schematic setup of the home made system for current vs. voltage measurements is shown.

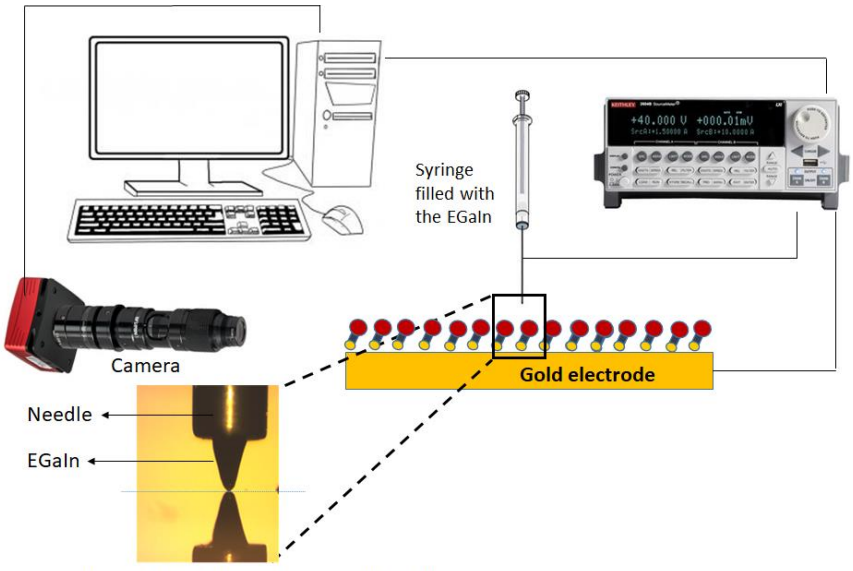

Real picture of the EGaIn cone contacting the monolayer on Au. The reflection of the cone can be seen.

4.6 Statistical Analysis of the measured IV curves.

For the statistical analysis of the I-V curves, we have employed the free R software. For doing so, we have taken into account that the trimmed mean values and standard deviations are robust estimators of central tendency. To compute a trimmed mean, a predetermined amount of observations is removed on each side of a distribution (remove outliers), and the remaining observations are averaged. Trimmed mean values provide a better estimation of the location of the bulk of the observations than a bare mean function when sampling from slightly asymmetric distributions. On the other hand, the bare standard deviation is dramatically affected by outliers and slightly asymmetries. More reliable results are obtained using the trimmed standard deviation. The trim argument can vary between 0 and 0.5. In this work, we have removed 10% of the total data, for which trim argument must be equal to 0.1. In this case, 5% of the upper part and 5% in the lower part is omitted.

To construct the histograms shown in Figure 6, we have considered two formulas to determine the number of bins in the histogram. We considered the Sturge's rule and the square root of the number of data ($\sqrt{N}$).

Sturge's rule is recommended when data is not skewed (as expected for Gaussian distribution). It should provide a good choice of bins in a histogram. In our data treatment, we follow roughly the Sturge's rule although for $N \leq 100$ there is no big differences in the number of bins compared to ($\sqrt{N}$). Importantly, the histograms are normalized to their area in order to analyze the data correctly. For instance, the function of density line is applied only when the data is normalized. Density line can be used as an assessment of your best histogram.

ANNEX I: SAMs characterization: Cyclic–square wave voltammetry, Electrochemical impedance spectroscopy, EPR, XPS, NEXAFS and charge transport using the EGaIn technique.

I.1 SAM on silicon surface characterization.

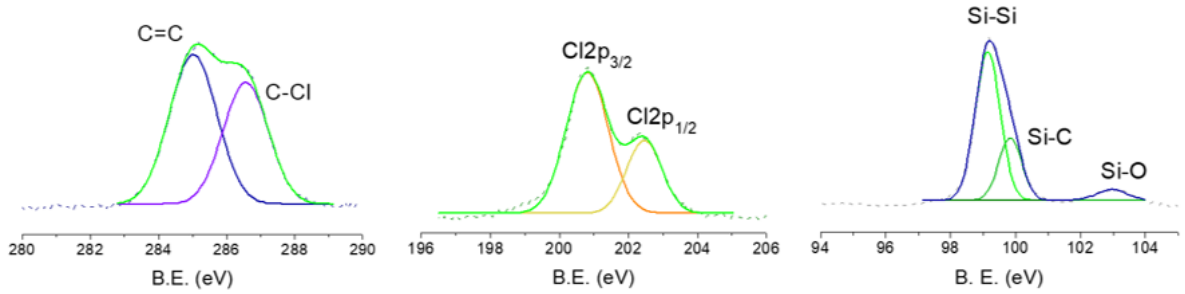

Figure S1: High-resolution XPS spectra deconvoluted peaks of **SAM-1-Rad-Si**: C 1s, Cl 2p and Si2p (from the left to the right).

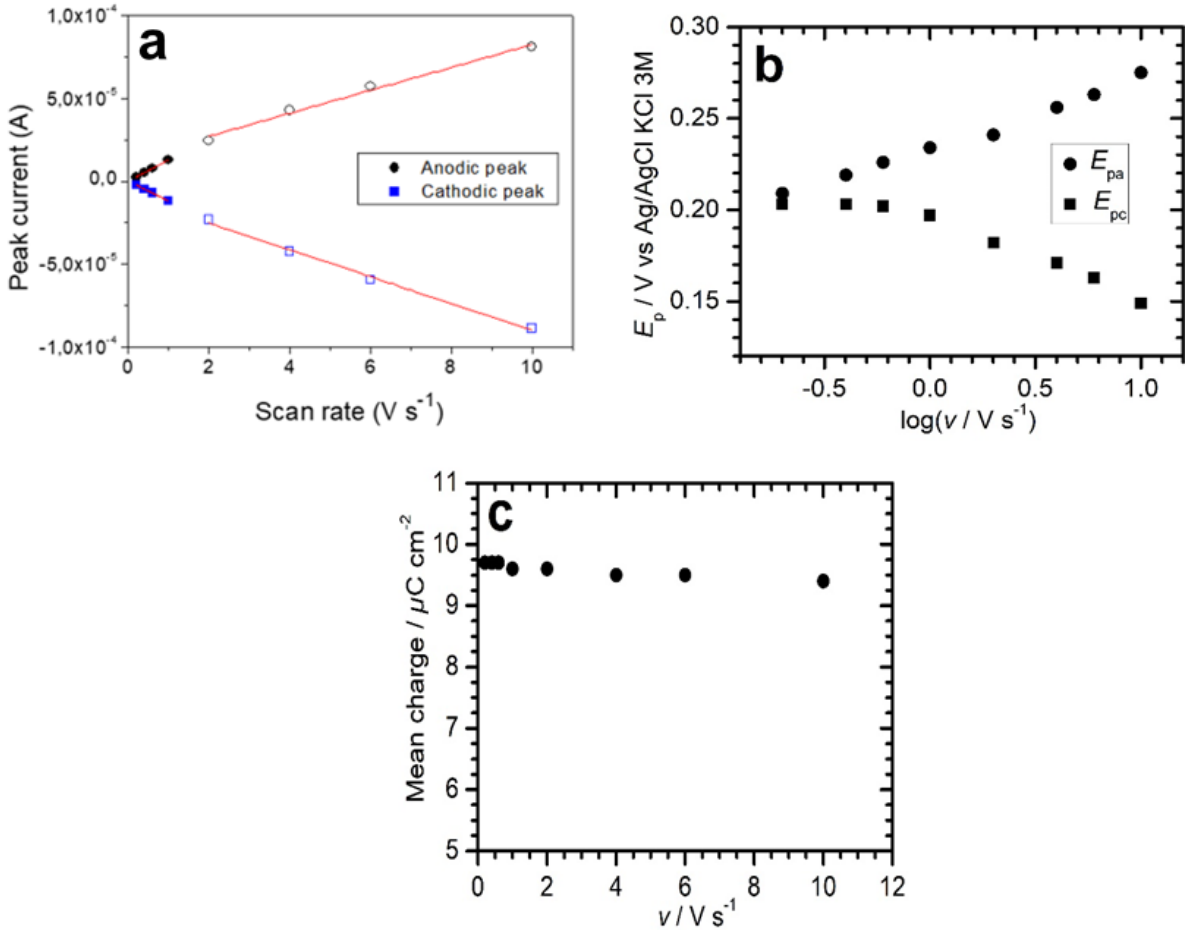

Figure S2: a) Anodic and cathodic peak photocurrent intensities plotted vs potential scan rate *v* under red-light illumination for **SAM-1-Rad-Si**, showing good linear relationships in the lower and higher scan rate ranges. b) Corresponding plots of the anodic E_{pa} and cathodic E_{pc} peak potentials as a function of log*v*. c) Mean charge (average of the anodic and cathodic charges calculated from the respective areas under the cyclic voltammetry peaks) vs *v* plot.

Mott-Schottky relationship (Equation S2):

$$\frac{1}{C_{sc}^2} = \frac{2}{eN_D A^2 \varepsilon_0 \varepsilon_r}\left(E - E_{fb} - \frac{kT}{e}\right) \qquad \text{Equation S2}$$

where:

- C_{SC} is the space charge capacitance;
- N_D is the the dopant density;
- E_{fb} is the flatband potential
- e is the electron charge (1.602 ×·10^{-19} C);
- ε_r is the relative permittivity of Si (11.7);
- ε_0 is the vacuum permittivity (8.85 ×·10^{-12} F m^{-1});
- A is the electrode surface area;
- E is the applied potential;
- k is the Boltzmann constant (1.38·× 10^{-23} m^2·kg·s^{-2}·K^{-1});
- T is temperature

N_D can be determined from the slope (b) of the linear part of the C_{SC}^{-2}-E plot (Figure S3) and E_{fb} is given by

$$E_{fb} = -\frac{a}{b} - \frac{kT}{e}$$

where a is the intercept of the linear part.

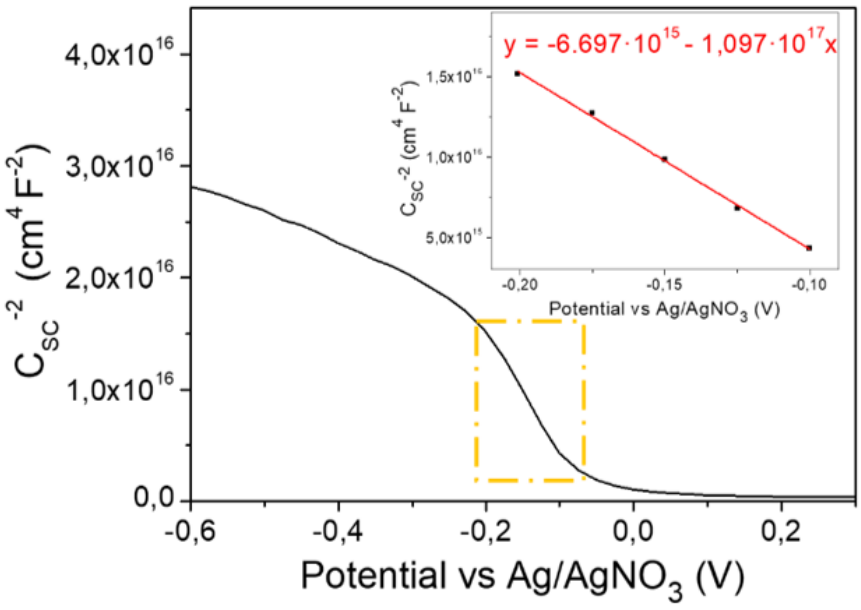

Figure S3: Mott-Schottky plot from impedance measurements at 50 kHz. The inset shows the linear fitting of the region indicated by the yellow rectangle.

I.2 SAM on gold surface characterization.

Figures S4 and S5 correspond to the on-surface modification of **SAM-2-Rad** using toluene as solvent. Figures S6 and S7 were obtained from the modification performed in acetonitrile. See above (page S14) for further details. Figure S8 corresponds to **SAM-3-Rad** and is used to extract a comparative Fc/PTM ratio.

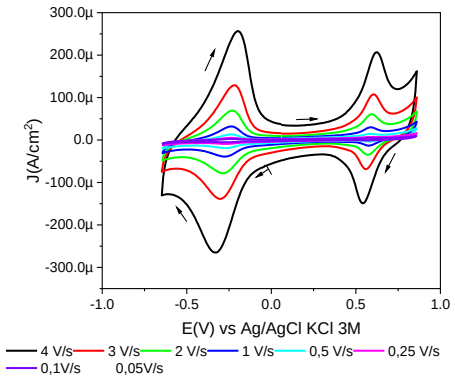

Figure S4: Cyclic voltammetry behaviour of **SAM-5-Rad**- using as electrolytic medium solution 0.1M $TBAPF_6$/ CH_2Cl_2, under argon atmosphere.

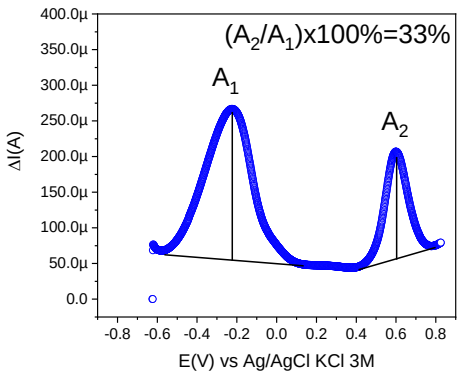

Figure S5: Square wave voltammetry behaviour of **SAM-5-Rad** using as electrolytic medium solution 0.1M $TBAPF_6$/ CH_2Cl_2, under argon atmosphere. Step=1mV, $E_{modulation}$=20mV and Frequency=100Hz

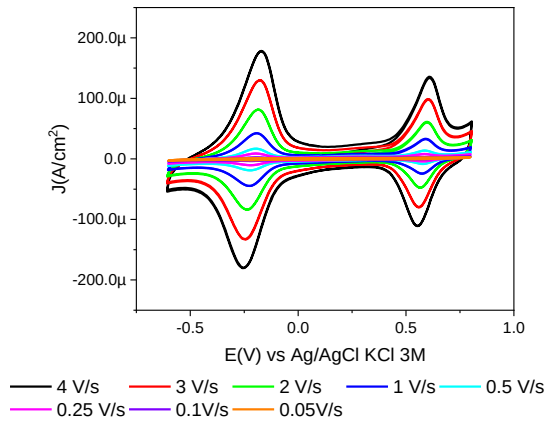

Figure S6: Cyclic voltammetry behaviour of **SAM-5-Rad** using as electrolytic medium solution 0.2M $TBAPF_6$/ CH_2Cl_2, under argon atmosphere.

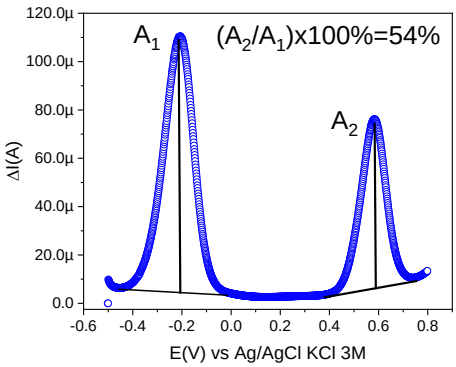

Figure S7: Square wave voltammetry behaviour of **SAM-5-Rad** using as electrolytic medium solution 0.2M $TBAPF_6$/ CH_2Cl_2, under argon atmosphere. Step=1mV, $E_{modulation}$=20mV and Frequency=40Hz

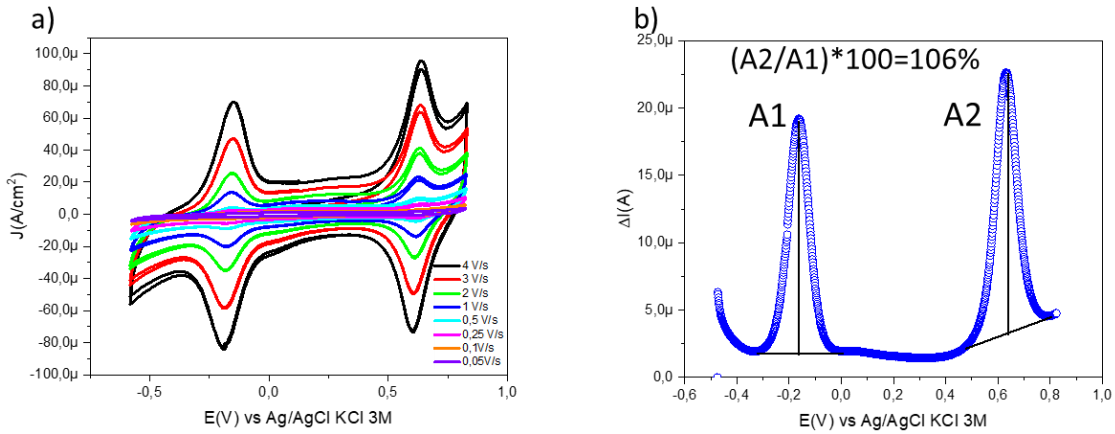

Figure S8: a) Cyclic voltammetry behaviour of **SAM-3-Rad** using as electrolytic medium solution 0.2M $TBAPF_6$/ CH_2Cl_2, under argon atmosphere, b) Square wave voltammetry behaviour of **SAM-3-Rad** using as electrolytic medium solution 0.2M $TBAPF_6$/ CH_2Cl_2, under argon atmosphere. Step=1mV, $E_{modulation}$=20mV and Frequency=40Hz

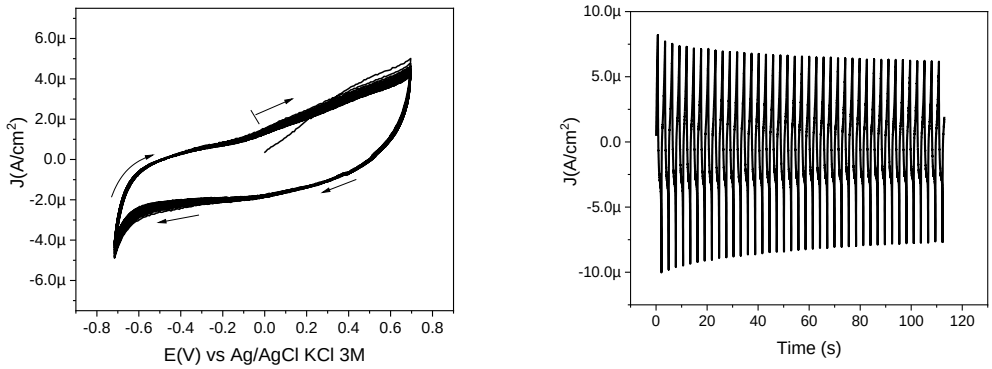

Figure S9: *Left:* Cyclic voltammetry (40 scans) of the blank Au ^{TS} (without the SAM) using as electrolytic medium solution 0.2M $TBAPF_6$/ CH_2Cl_2, under argon atmosphere and as scan rate 1V/s. *Right:* Current intensity stability over time.

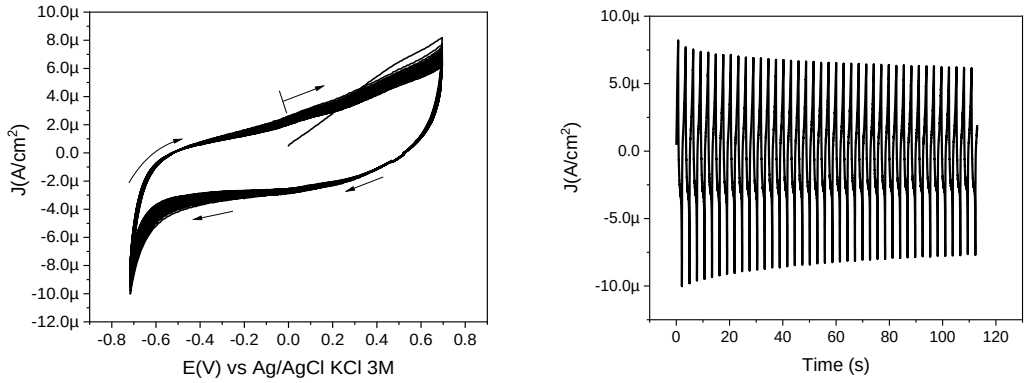

Figure S10: *Left:* Cyclic voltammetry (40 scans) of **SAM-2-H** using as electrolytic medium solution 0.2M $TBAPF_6$/ CH_2Cl_2, under argon atmosphere and as scan rate 1V/s. *Right:* Current density stability over time.

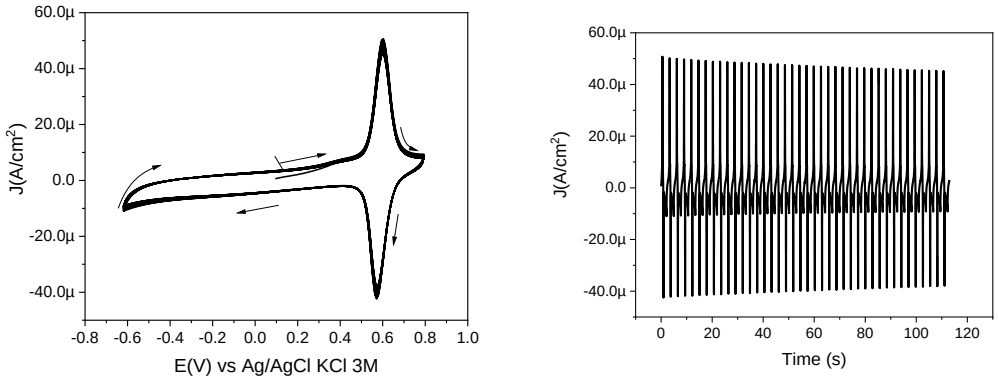

Figure S11 *Left:* Cyclic voltammetry (40 scans) of **SAM-3-H** using as electrolytic medium solution 0.2M $TBAPF_6$/ CH_2Cl_2, under argon atmosphere and as scan rate 1V/s. *Right:* Current density stability over time.

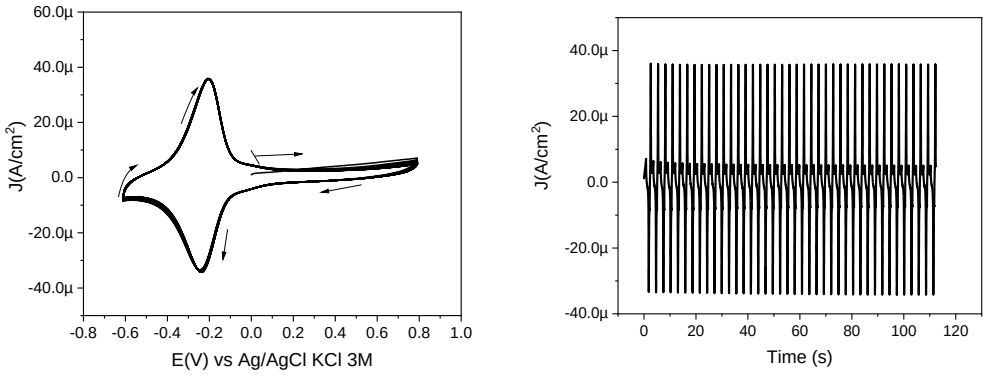

Figure S12: *Left:* Cyclic voltammetry (40 scans) of **SAM-2-Rad** using as electrolytic medium solution 0.2M $TBAPF_6$/ CH_2Cl_2, under argon atmosphere and as scan rate 1V/s. *Right:* Current density stability over time.

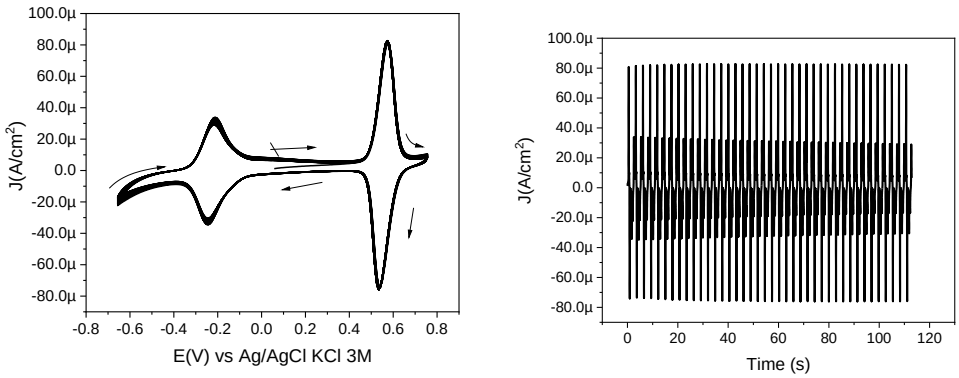

Figure S13: *Left:* Cyclic voltammetry behaviour (40 scans) of **SAM-3-Rad** using as electrolytic medium solution 0.2M $TBAPF_6$/ CH_2Cl_2, under argon atmosphere and as scan rate 1V/s. *Right:* Current density stability over time.

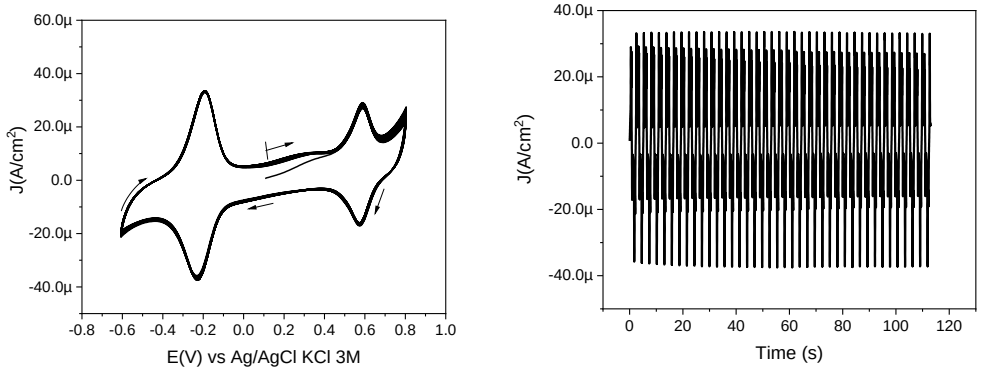

Figure S14: *Left:* Cyclic voltammetry (40 scans) of **SAM-5-Rad** using as electrolytic medium solution 0.2M $TBAPF_6/CH_2Cl_2$, under argon atmosphere and as scan rate 1V/s. *Right:* Current density stability over time.

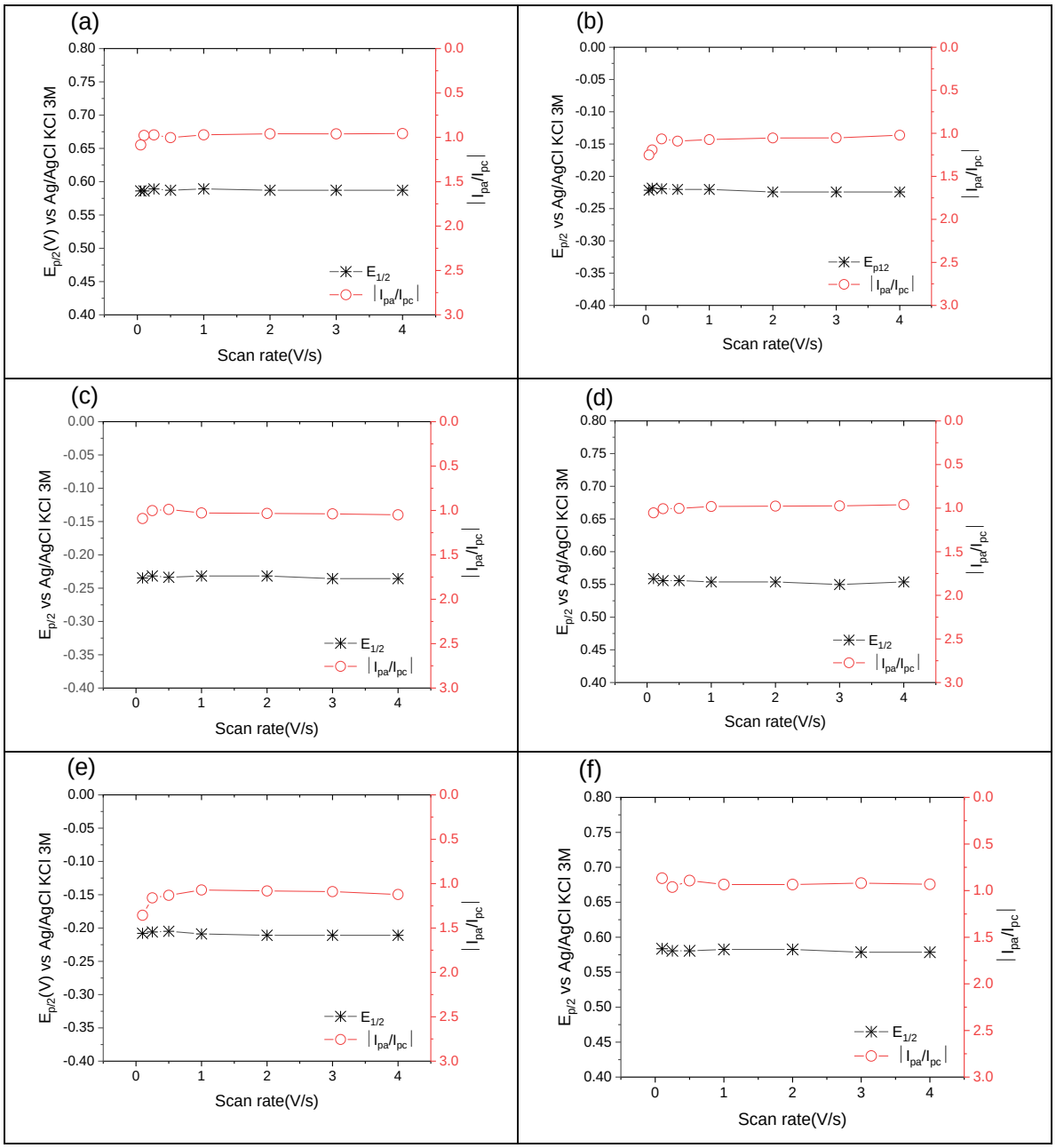

Figure S15: Plots of $E_{1/2}$ and $|I_{pa}/I_{pc}|$ versus scan rate for a) **SAM-3-H** d) **SAM-3-Rad** f) **SAM-5-Rad** (for the Fc peaks), and b) **SAM-2-Rad** c) **SAM-3-Rad** e) **SAM-5-Rad** (for the PTMs radical peaks).

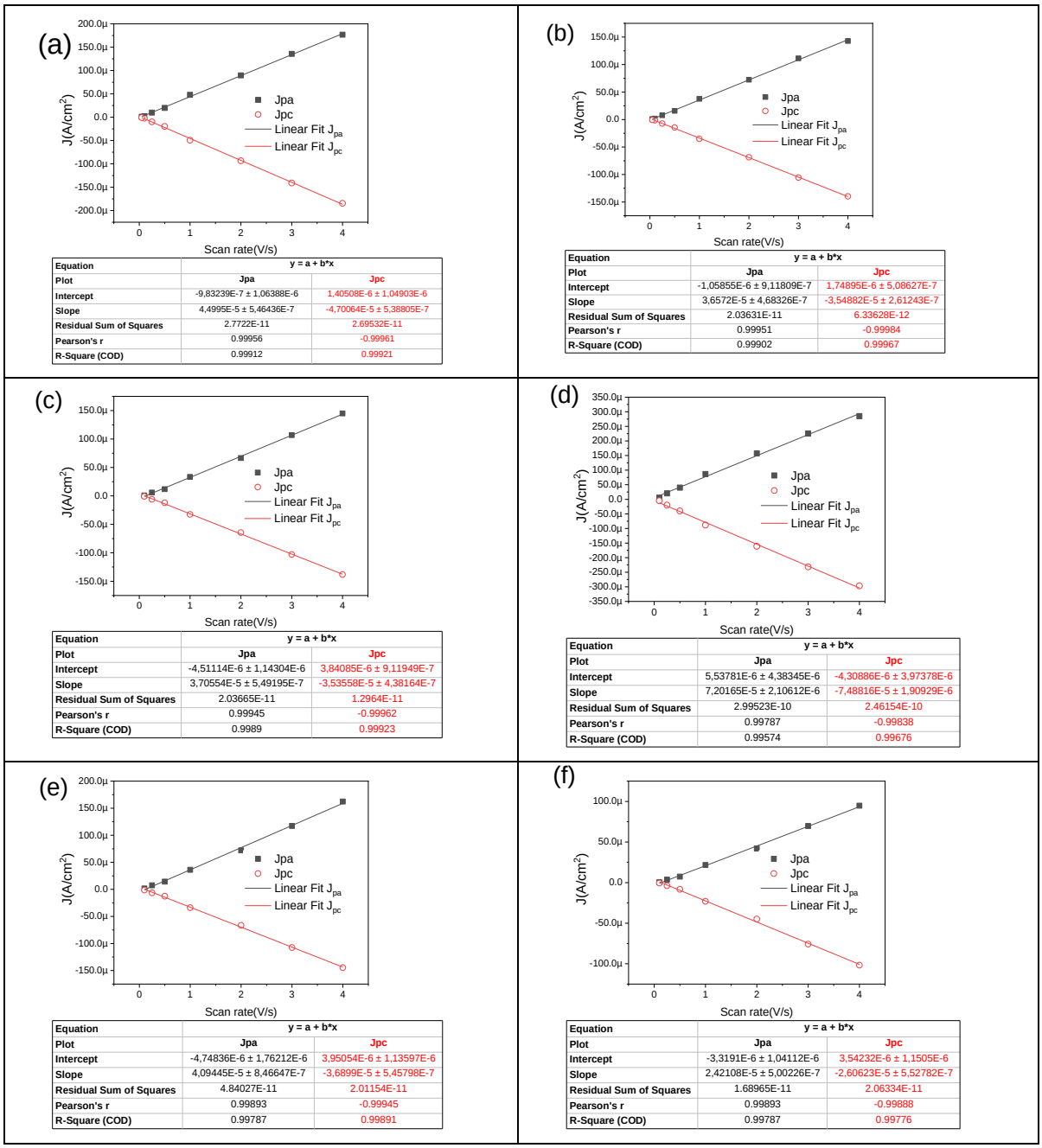

Equation	y = a + b*x	
Plot	Jpa	Jpc
Intercept	-9,83239E-7 ± 1,06388E-6	1,40508E-6 ± 1,04903E-6
Slope	4,4995E-5 ± 5,46436E-7	-4,70064E-5 ± 5,38805E-7
Residual Sum of Squares	2.7722E-11	2.69532E-11
Pearson's r	0.99956	-0.99961
R-Square (COD)	0.99912	0.99921

Equation	y = a + b*x	
Plot	Jpa	Jpc
Intercept	-1,05855E-6 ± 9,11809E-7	1,74895E-6 ± 5,08627E-7
Slope	3,6572E-5 ± 4,68326E-7	-3,54882E-5 ± 2,61243E-7
Residual Sum of Squares	2.03631E-11	6.33628E-12
Pearson's r	0.99951	-0.99984
R-Square (COD)	0.99902	0.99967

Equation	y = a + b*x	
Plot	Jpa	Jpc
Intercept	-4,51114E-6 ± 1,14304E-6	3,84085E-6 ± 9,11949E-7
Slope	3,70554E-5 ± 5,49195E-7	-3,53558E-5 ± 4,38164E-7
Residual Sum of Squares	2.03665E-11	1.2964E-11
Pearson's r	0.99945	-0.99962
R-Square (COD)	0.9989	0.99923

Equation	y = a + b*x	
Plot	Jpa	Jpc
Intercept	5,53781E-6 ± 4,38345E-6	-4,30886E-6 ± 3,97378E-6
Slope	7,20165E-5 ± 2,10612E-6	-7,48816E-5 ± 1,90929E-6
Residual Sum of Squares	2.99523E-10	2.46154E-10
Pearson's r	0.99787	-0.99838
R-Square (COD)	0.99574	0.99676

Equation	y = a + b*x	
Plot	Jpa	Jpc
Intercept	-4,74836E-6 ± 1,76212E-6	3,95054E-6 ± 1,13597E-6
Slope	4,09445E-5 ± 8,46647E-7	-3,6899E-5 ± 5,45798E-7
Residual Sum of Squares	4.84027E-11	2.01154E-11
Pearson's r	0.99893	-0.99945
R-Square (COD)	0.99787	0.99891

Equation	y = a + b*x	
Plot	Jpa	Jpc
Intercept	-3,3191E-6 ± 1,04112E-6	3,54232E-6 ± 1,1505E-6
Slope	2,42108E-5 ± 5,00226E-7	-2,60623E-5 ± 5,52782E-7
Residual Sum of Squares	1.68965E-11	2.06334E-11
Pearson's r	0.99893	-0.99888
R-Square (COD)	0.99787	0.99776

Figure S16: Plots of anodic and cathodic current densities versus scan rate. a) **SAM-3-H** d) **SAM-3-Rad** f) **SAM-5-Rad** (for the Fc peaks), and b) **SAM-2-Rad** c) **SAM-3-Rad** e) **SAM-5-Rad** (for the PTMs radical peaks).

Table S2. Surface coverage of SAMs calculated with Equation 1 for the different SAMs studied here.

Sample	*Γ (mol cm^{-2}) PTM Radical*	*Γ (mol cm^{-2}) Ferrocene*
SAM-3-H	--	5.8 x 10^{-11}
SAM-2-Rad	8.9 x 10^{-11}	--
SAM-3-Rad	7.9 x 10^{-11}	1.0 x 10^{-10}
SAM-5-Rad	8.6 x 10^{-11}	4.0 x 10^{-11}

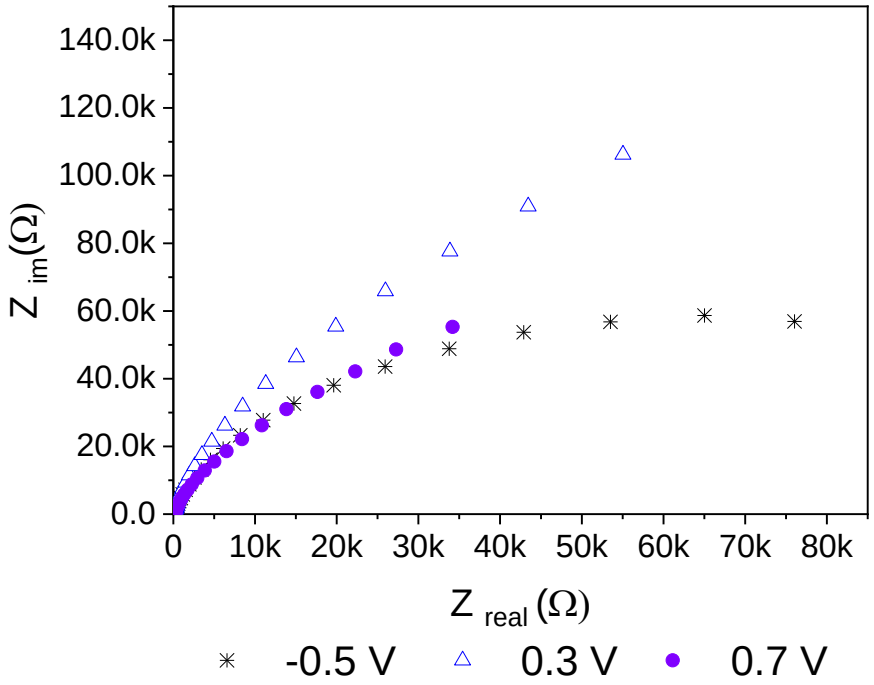

Figure S17: Impedance Nyquist plots for three applied potentials of the **SAM-3-Rad** using 0.1M $TBAPF_6/CH_2Cl_2$ as the electrolytic medium under argon atmosphere and a scan frequency from 100 kHz to 0.1 Hz with 20 mV amplitude.

XPS and NEXAFS Characterization of the SAMs

Stoichiometric and experimental elemental ratios for SAM-3-Rad. The values were obtained as discussed in reference[12].

Table S3. Stoichiometric and experimental elemental ratios for **SAM-3-Rad**.

	C	**N**	**Cl**	**Fe**
Sensitivity factor*	0.25	0.42	0.73	3
Number of atoms	50	3	13	1
Theoretical values (%)	75	4	19	2
SAM-3-Rad (%)	84.3	5.2	10.0	0.5

Stoichiometric and experimental elemental ratios for SAM-2-Rad.

Table S4. Stoichiometric and experimental elemental ratios for **SAM-2-Rad**.

	C	**Cl**
Sensitivity factor*	0.25	0.73
Number of atoms	39	13
Theoretical values (%)	75	25
SAM-2-Rad (%)	95	5

Stoichiometric and experimental elemental ratios for SAM-5-Rad.

Table S5. Stoichiometric and experimental elemental ratios for **SAM-5-Rad**.

	C	**N**	**Cl**	**Fe**
Sensitivity factor*	0.25	0.42	0.73	3
Number of atoms	50	3	13	1
Theoretical values (%)	75	4	19	2
SAM-5-Rad (%)	83.9	5.8	10.1	0.2

* C. D. Wagner, *J. Electron Spectrosc. Relat. Phenom.* **1983**, *32*, 99-102.

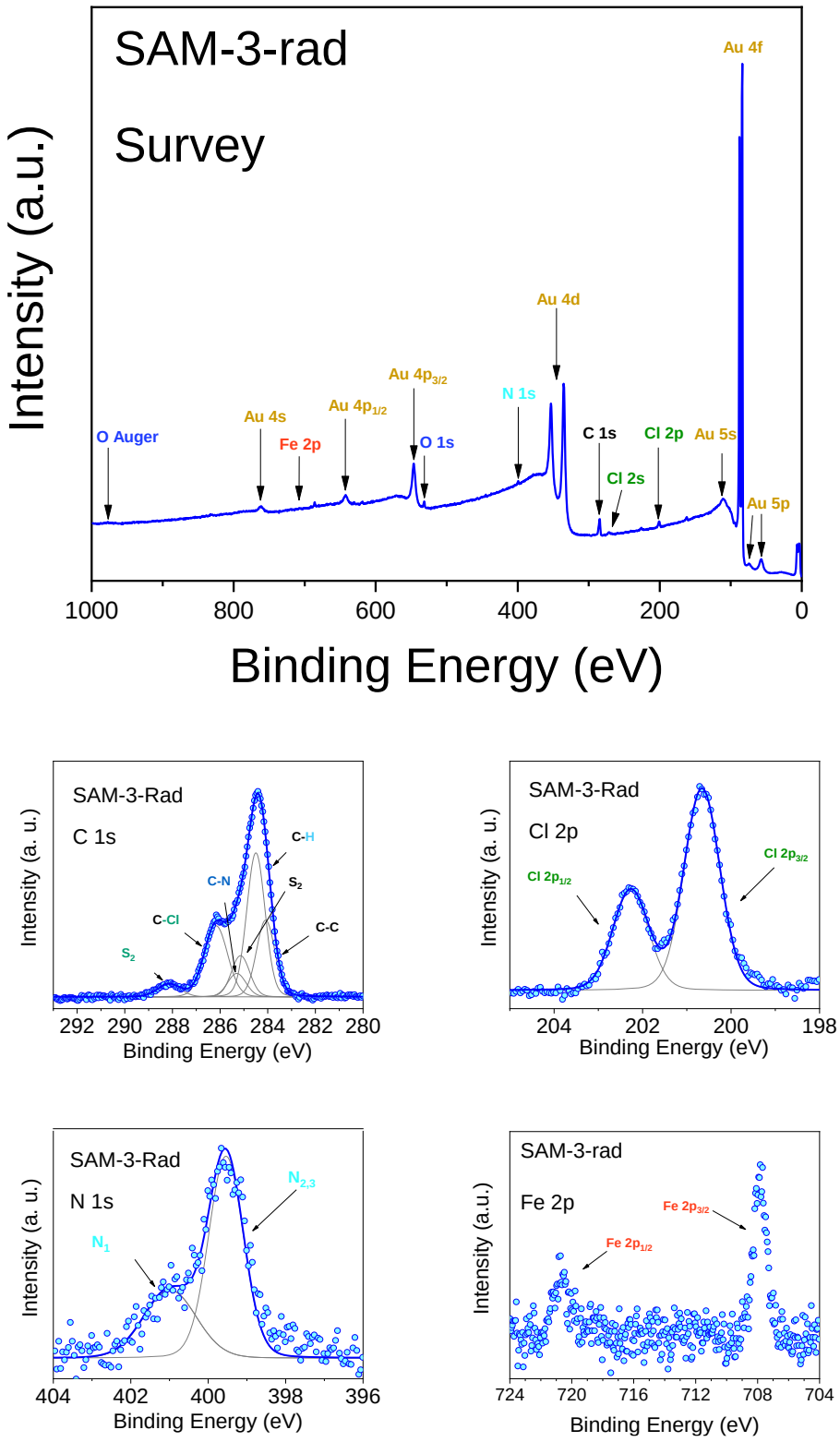

Figure S18: (upper panel) Survey and (lower panels) C 1s, Cl 2p, N 1s (together with their best fit) and Fe 2p XPS spectra of **SAM-3-Rad** (photon energy = 1486.6 eV).

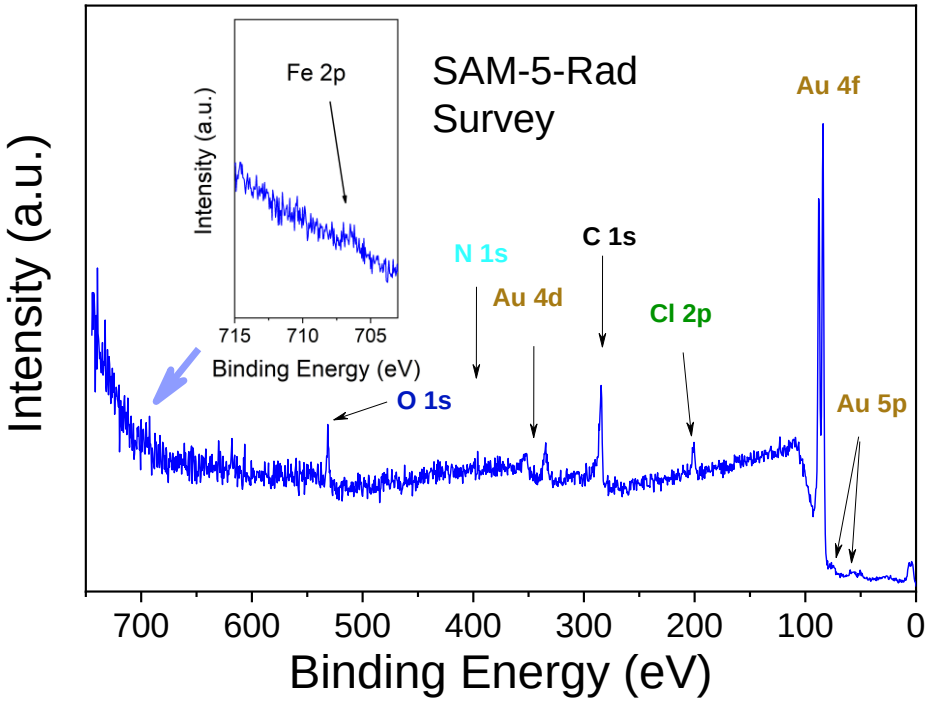

Figure S19: XPS survey spectrum of **SAM-5-Rad** together with the detailed Fe 2p core level spectrum (photon energy = 800 eV)

We used Voigt profiles, with fixed constant Lorentzian width. The Voigt profile considers both the finite core-hole lifetime (Lorentzian profile) and the broadening due to the finite experimental resolution and various inhomogeneities, e.g., molecular packing and local morphology[13,14] (Gaussian profile). To calculate the stoichiometry of the films, we also considered the intensity of the satellites[14,15], typical features in photoemission that appear as an effect of the relaxation processes due to the creation of a core-hole[16]. The fit that we use is based on the procedure adopted for closed-shell molecules[14]. The final fit is the result of several self-consistent interactions of sequential fits done considering all physical and chemical information and adding more constraints at each interaction, with the goal to keep the parameter dependency very low.

As we were more interested in the stoichiometry than in physical phenomena related to photoemission, we kept the number of satellites as low as possible to have a very simplified fit. However, satellite intensities cannot be neglected, especially in case of radicals because the simultaneous presence of a core-hole and a singly occupied molecular orbital on the time-scale of photoemission enhances the relaxation phenomena.[17,18]

The fit procedure systematically holds for all samples of a specific molecule, prepared and measured under the same conditions. In this way, we can also identify the samples that do not correspond to the expected stoichiometry. We work on sets of measured samples that are big enough to be statistically significant. We obtain an excellent agreement between the theoretical and the fit values that indicates that **SAM-3-Rad** is close to the theoretical stoichiometry, while this is not the case for **SAM-5-Rad**, as discussed in the paper.

Table S6. Fit results for the energy positions and relative intensities of the photoemission lines in the C 1s spectra.

	Energy (eV)	**Lorentzian Width (eV)**	**Gaussian Width (eV)**	**Intensity (%)**	**Theoretical values (%)**
C-C	284.1	0.08	0.86	19.6	22
C-H	284.5	0.08	0.86	36.9	46
S_1	285.1	0.08	0.86	10.6	
C-N	285.3	0.08	0.87	6.0	6
C-Cl	286.2	0.08	1.10	22.9	26
S_2	288.1	0.08	1.10	4.0	

$I(C\text{-}C + C\text{-}H + S_1) = 67.1\ \%$

$I(C\text{-}Cl + S_2) = 26.9\ \%$

Table S7. Fit results for the energy positions and relative intensities of the photoemission lines in the Cl 2p spectra.

	Energy (eV)	**Lorentzian Width* (eV)**	**Gaussian Width (eV)**	**Intensity (%)**
Cl $2p_{3/2}$	200.7	0.1	0.9	66.3
Cl $2p_{3/2}$	202.3	0.1	0.9	33.7

*O. Travnikova et. al. *Chem. Phys. Lett.* **2006**, *426*, 452-458.

Table S8. Fit results for the energy positions and relative intensities of the photoemission lines in the N 1s spectra.

	Energy (eV)	Lorentzian Width (eV)	Gaussian Width (eV)	Intensity (%)
$N_{2,3}$	399.5	0.1	1,01	66.4
N_1	401.0	0.1	1.54	33.6

ANEX II: H^1-NMR, C^{13}-NMR, FT-IR, UV-Vis, LDI-TOF, EPR spectra and cyclic –square wave voltammetry of the synthesized molecules.

1) α-H-bisalkPTM-Fc_1 (3-H)

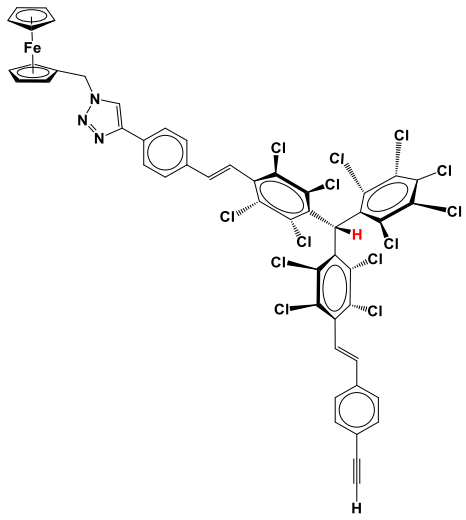

^{1}H-NMR, $CDCl_3$, 600 MHz

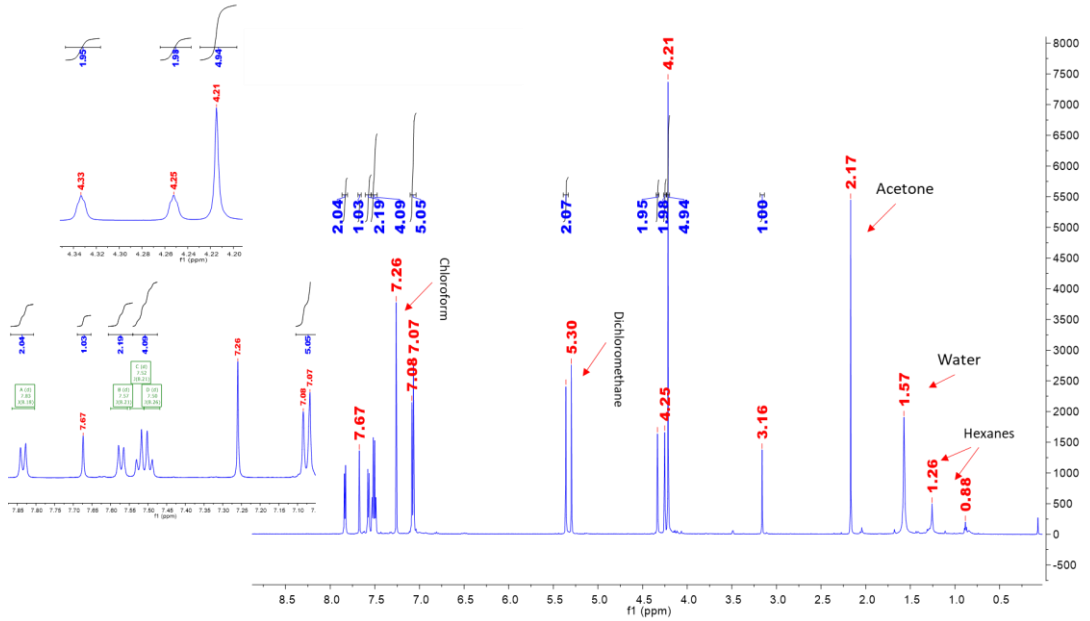

Figure S20: ^{1}H-NMR spectrum of **3-H** in $CDCl_3$.

^{13}C-NMR, $CDCl_3$, 101 MHz

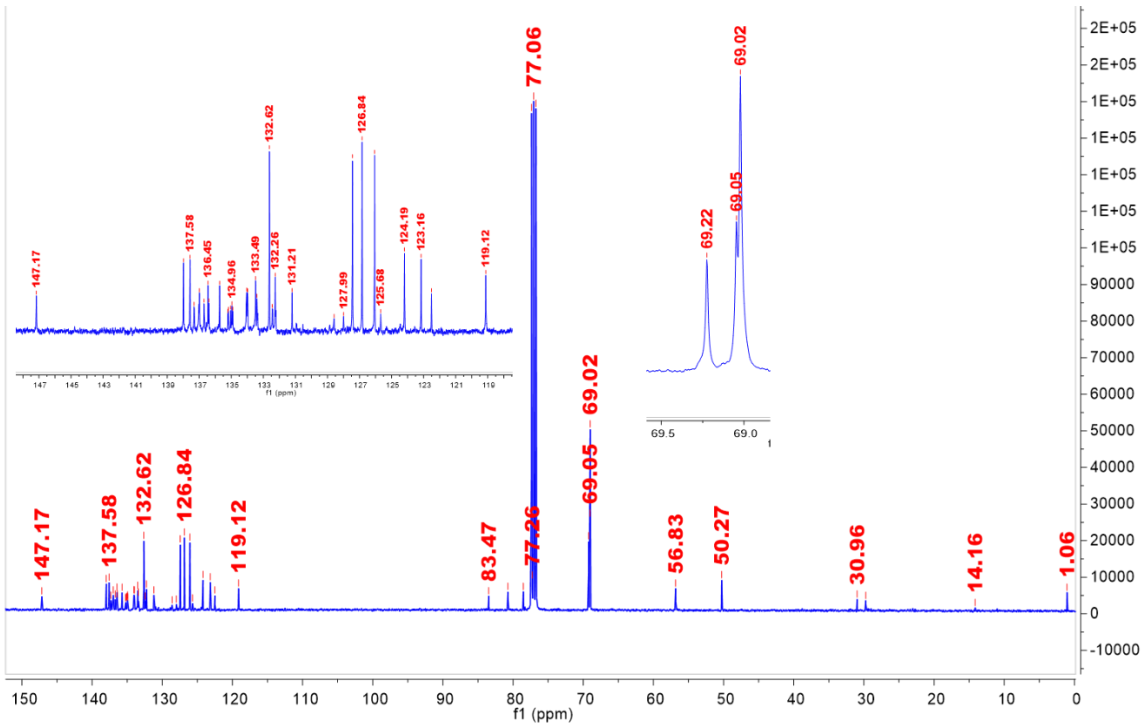

Figure S21: ^{13}C-NMR spectrum of **3-H** in $CDCl_3$

FT-IR

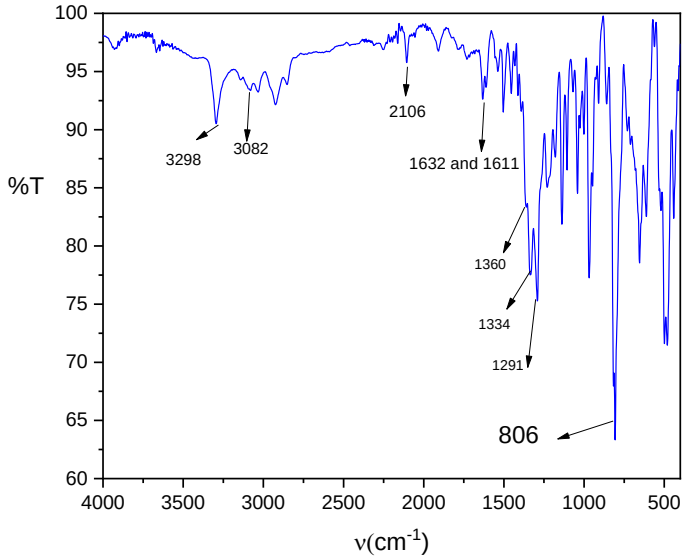

Figure S22: FT-IR spectrum of **3-H** in powder.

UV-Vis

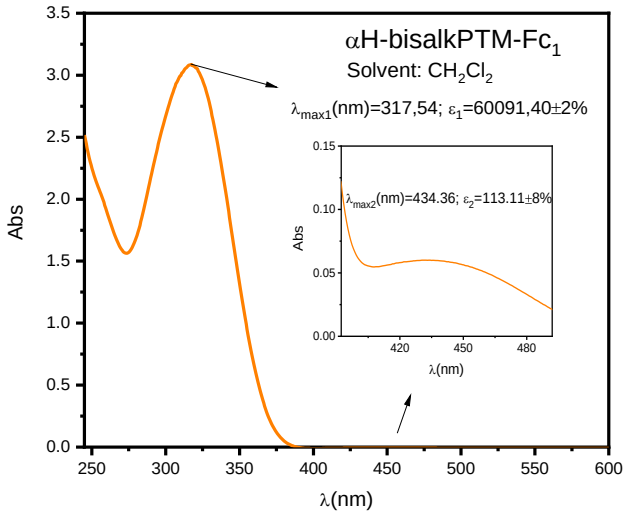

Figure S23: UV-Vis spectrum of **3-H** in CH_2Cl_2.

Cyclic voltammetry

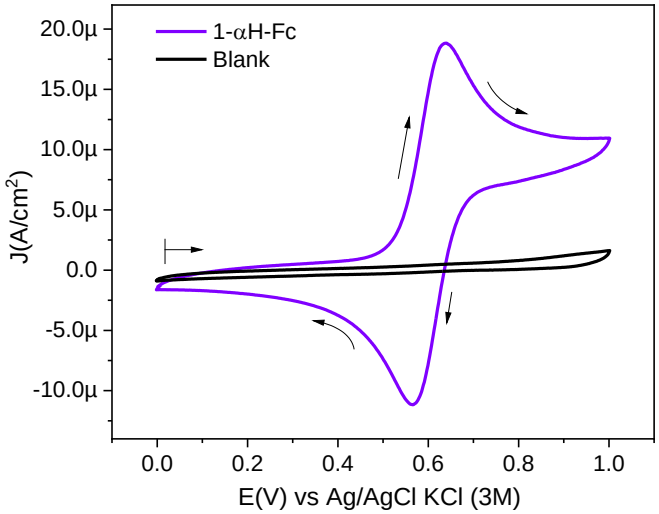

Figure S24: Cyclic Voltammetry of **3-H** at 0.5 mM over a glassy carbon electrode at 100mV/s, using as electrolytic medium a 0.1M solution of $TBAPF_6$ in CH_2Cl_2, under argon atmosphere.

MALDI-ToF

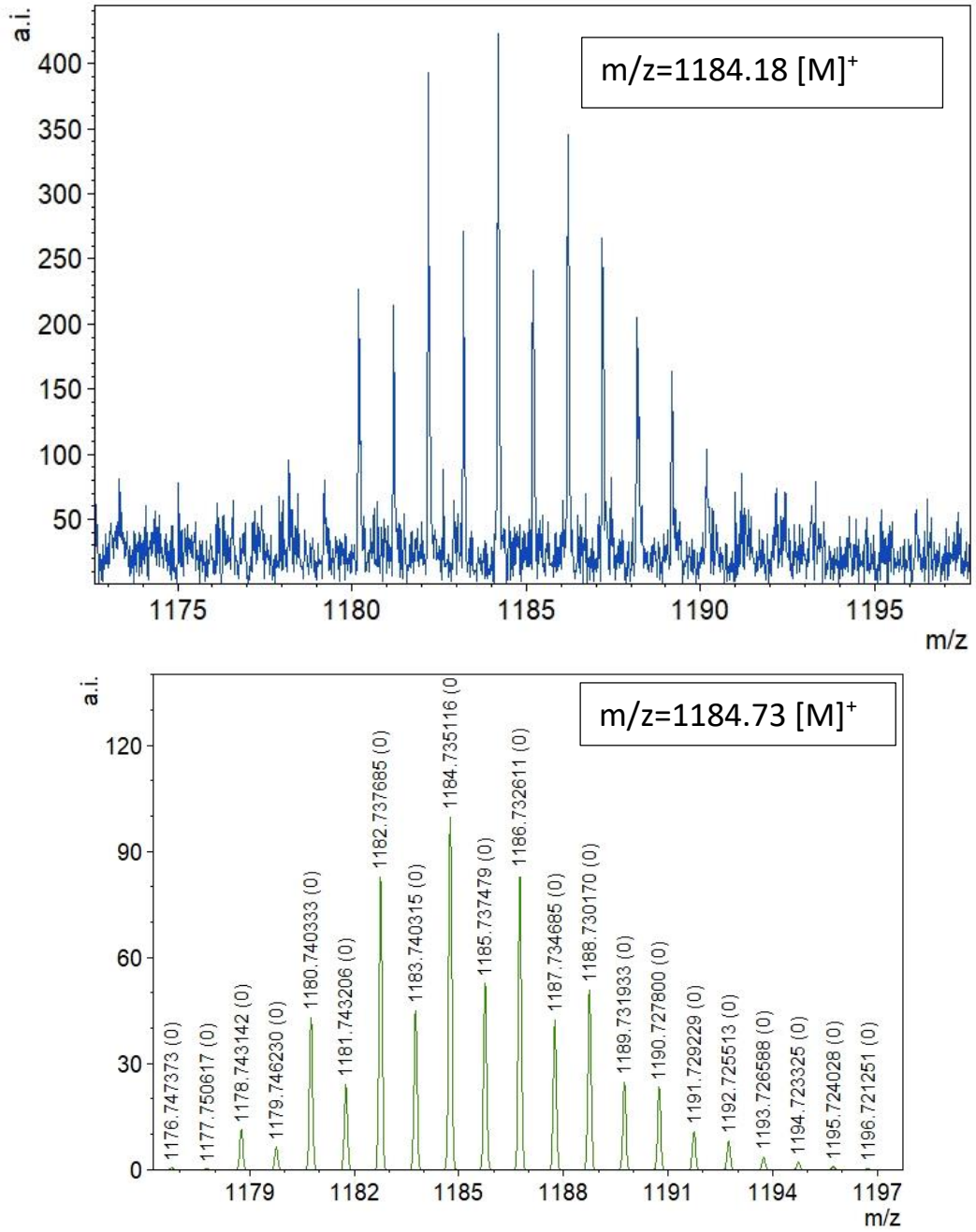

Figure S25: MALDI-ToF spectra of **3-H** experimental (top) and simulated (bottom)

α-H-bisalkPTM-Fc$_2$ (4-H)

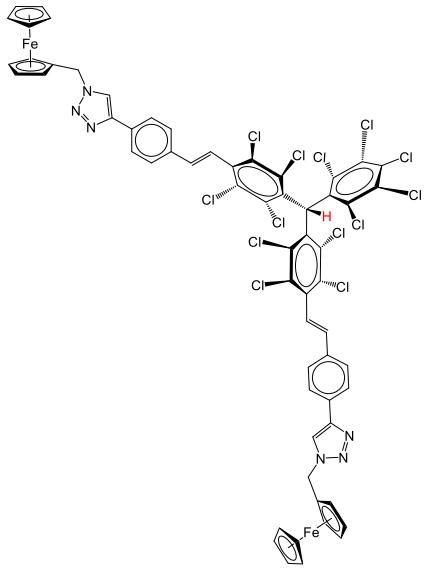

^{1}H-NMR, CDCl$_3$, 600 MHz

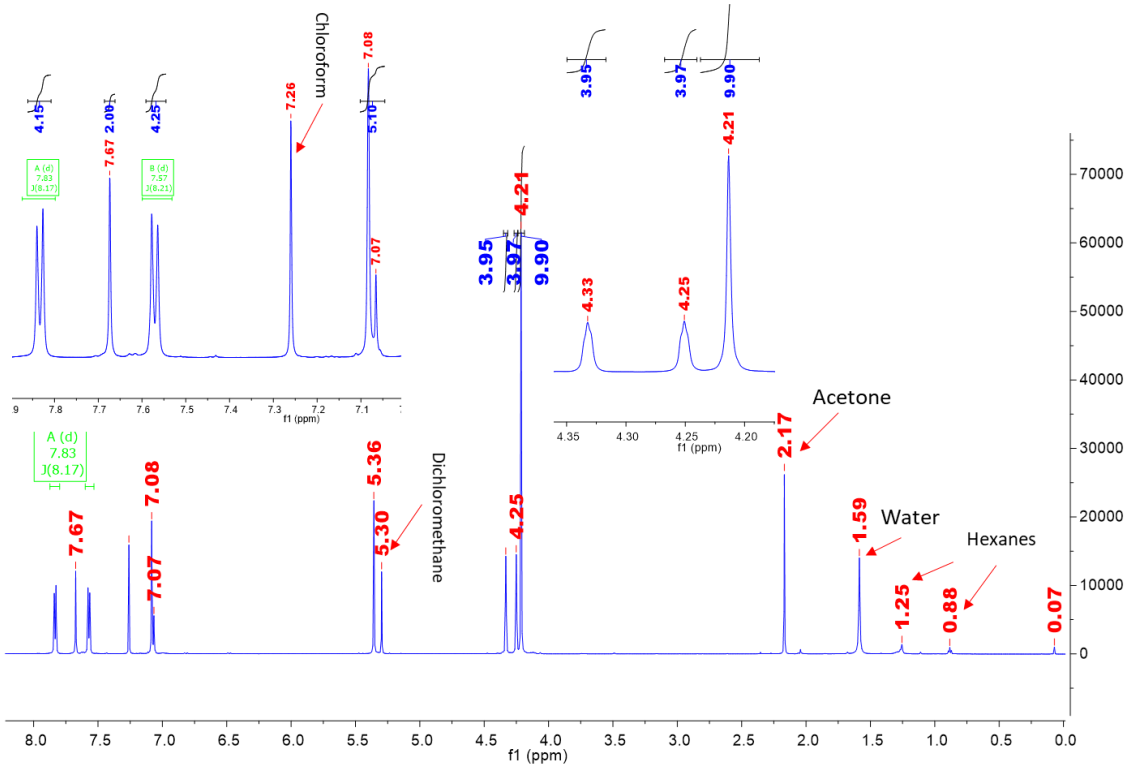

Figure S26: ^{1}H-NMR spectrum of **4-H** in CDCl$_3$.

^{13}C-NMR, $CDCl_3$, 101 MHz

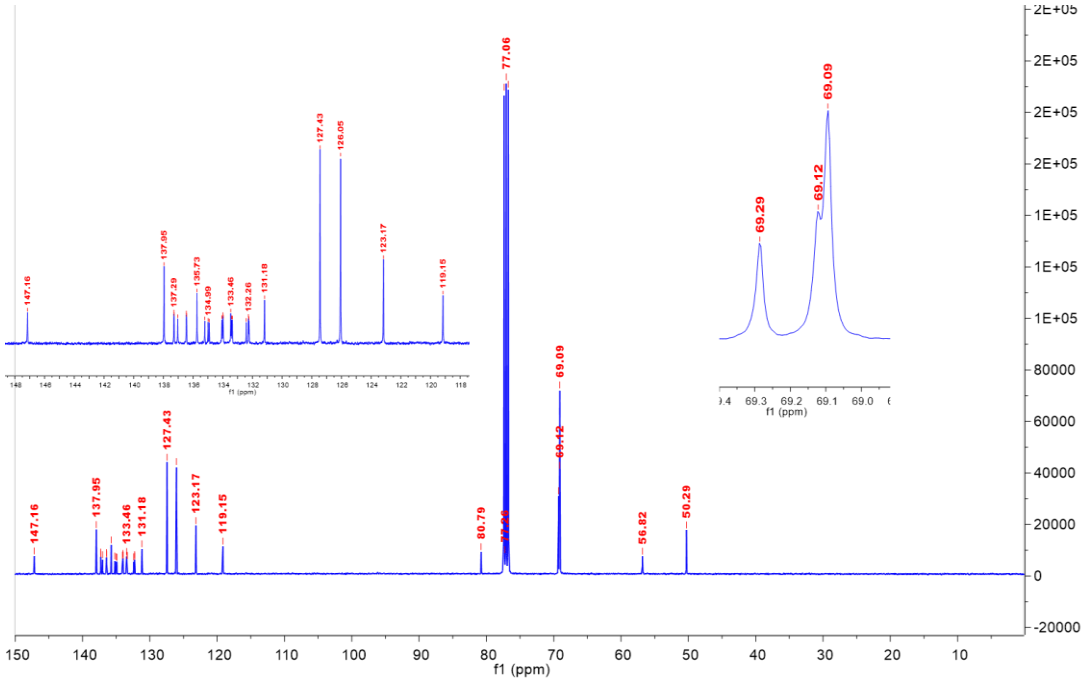

Figure S27: ^{13}C-NMR spectrum of **4-H** in $CDCl_3$.

FT-IR

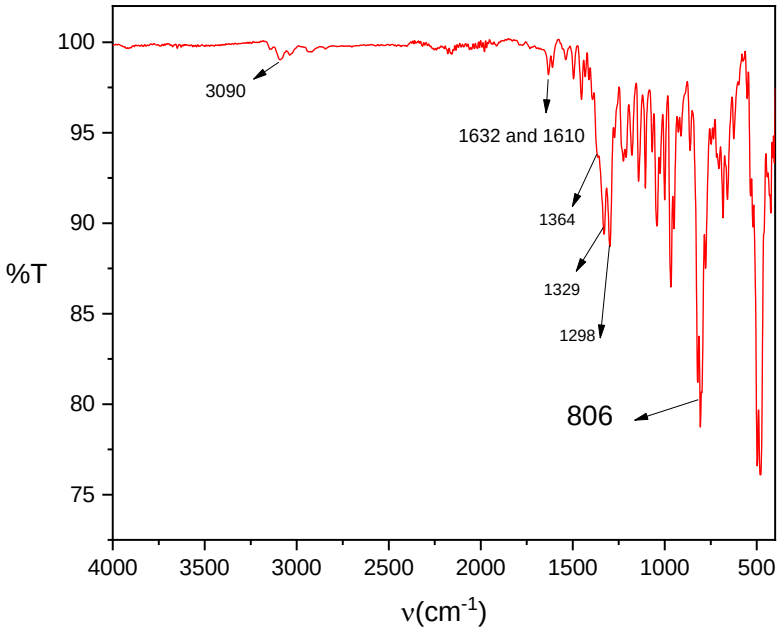

Figure S28: FT-IR spectrum of **4-H** in powder.

UV-Vis

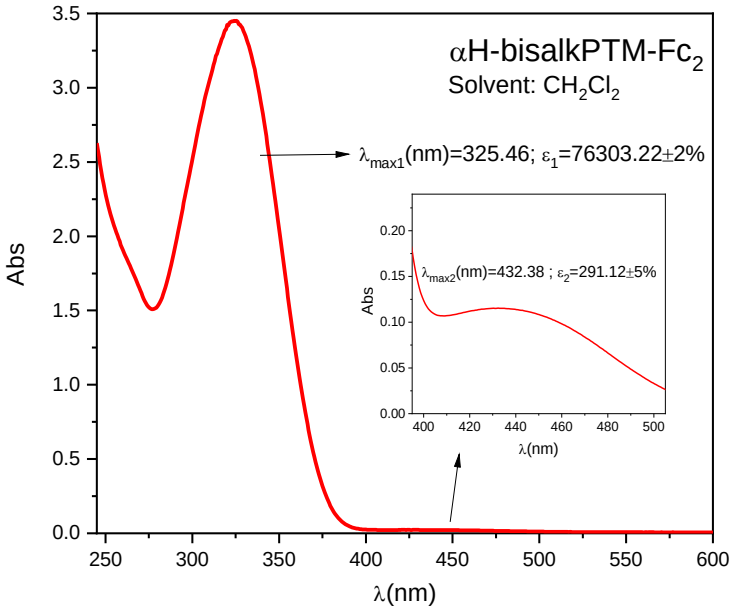

Figure S29: UV-Vis spectrum of **4-H** in CH_2Cl_2.

Cyclic voltammetry.

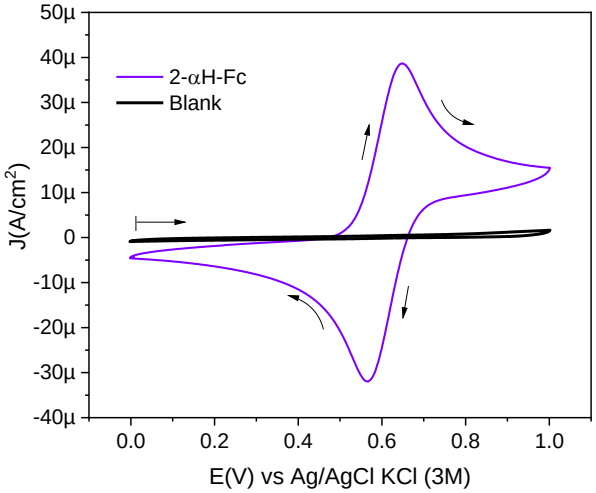

Figure S30: Cyclic Voltammetry of **4-H** at 0.46 mM over a glassy carbon electrode at 100mV/s, using as electrolytic medium a 0.1M solution of $TBAPF_6$ in CH_2Cl_2, under argon atmosphere.

MALDI-ToF

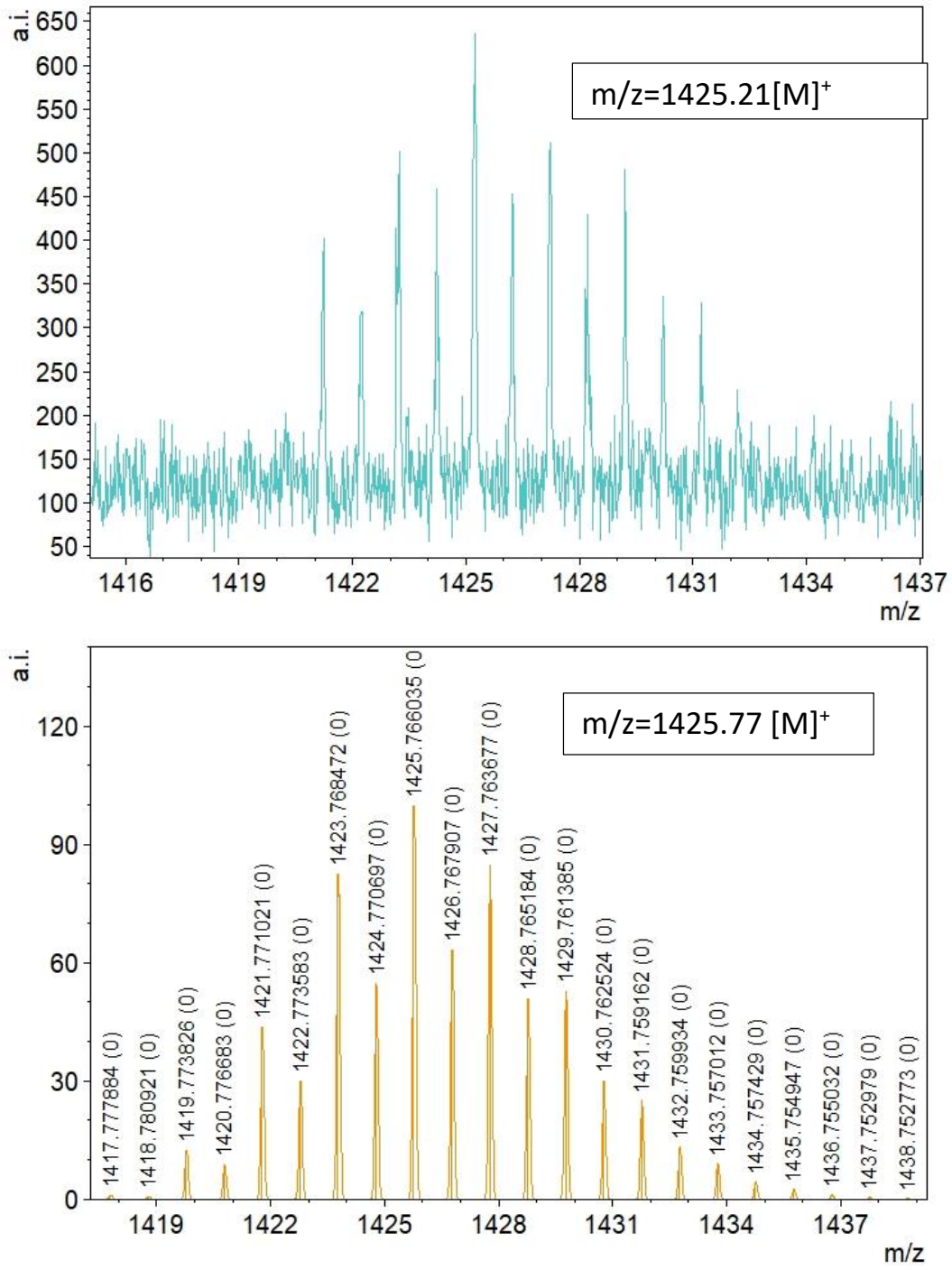

Figure S31: MALDI-ToF spectra of **4-H** experimental (top) and simulated (bottom).

rad-bisalkPTM-Fc$_1$ (3-Rad)

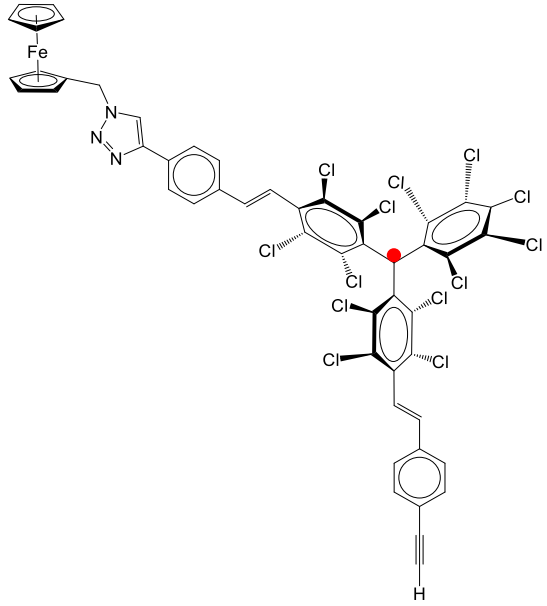

FT-IR

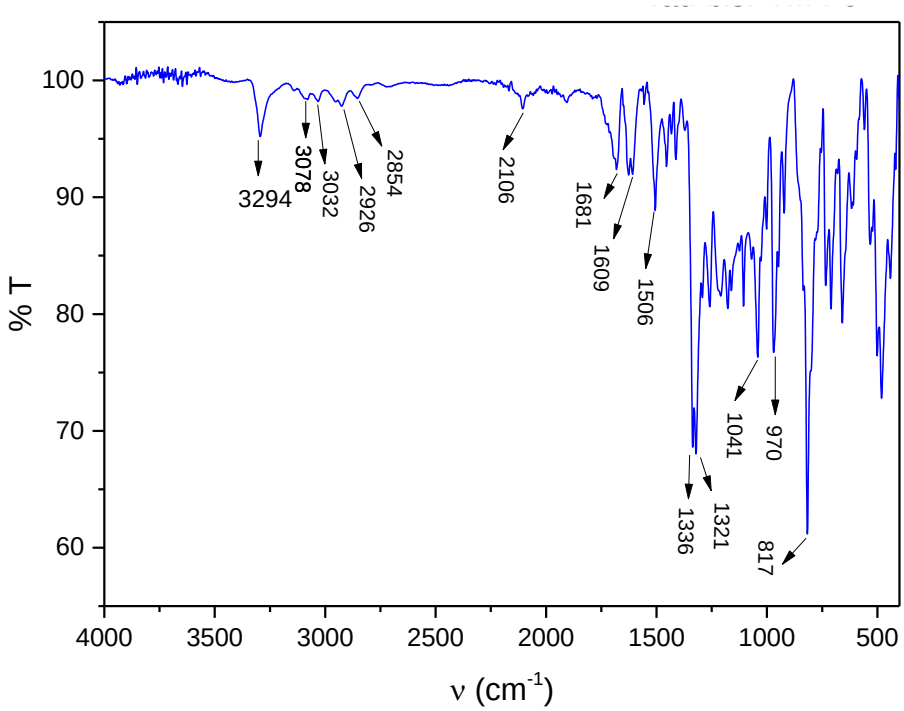

Figure S32: FT-IR spectrum of **3-Rad** in powder.

UV-Vis

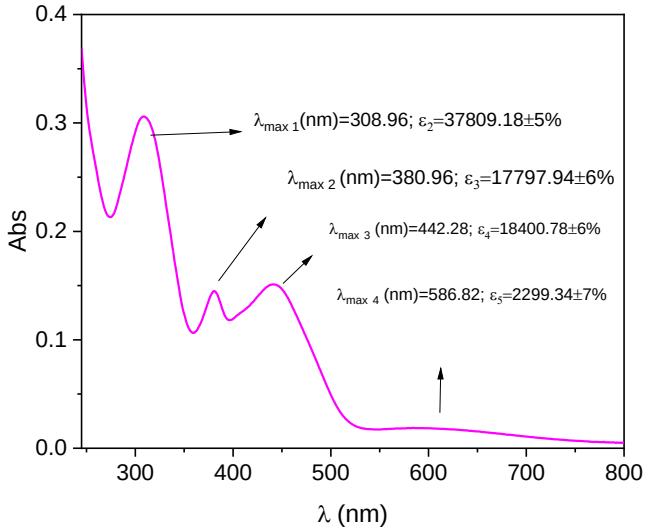

Figure S33: UV-Vis spectrum of **3-Rad** in CH_2Cl_2.
λ_{max} = maximum wavelength and ε= Molar absorptivity.

Electron paramagnetic resonance (EPR)

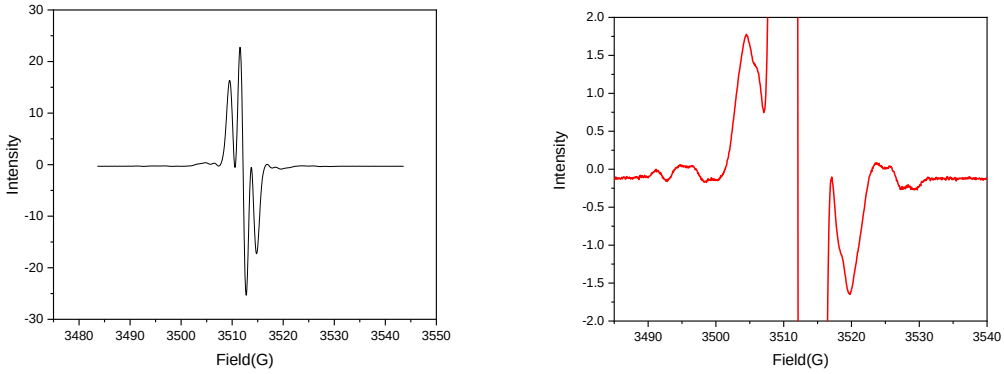

Figure S34: EPR spectra of **3-Rad** in dichloromethane at room temperature. The red spectrum (right) was recorded at higher power conditions.

MALDI-ToF

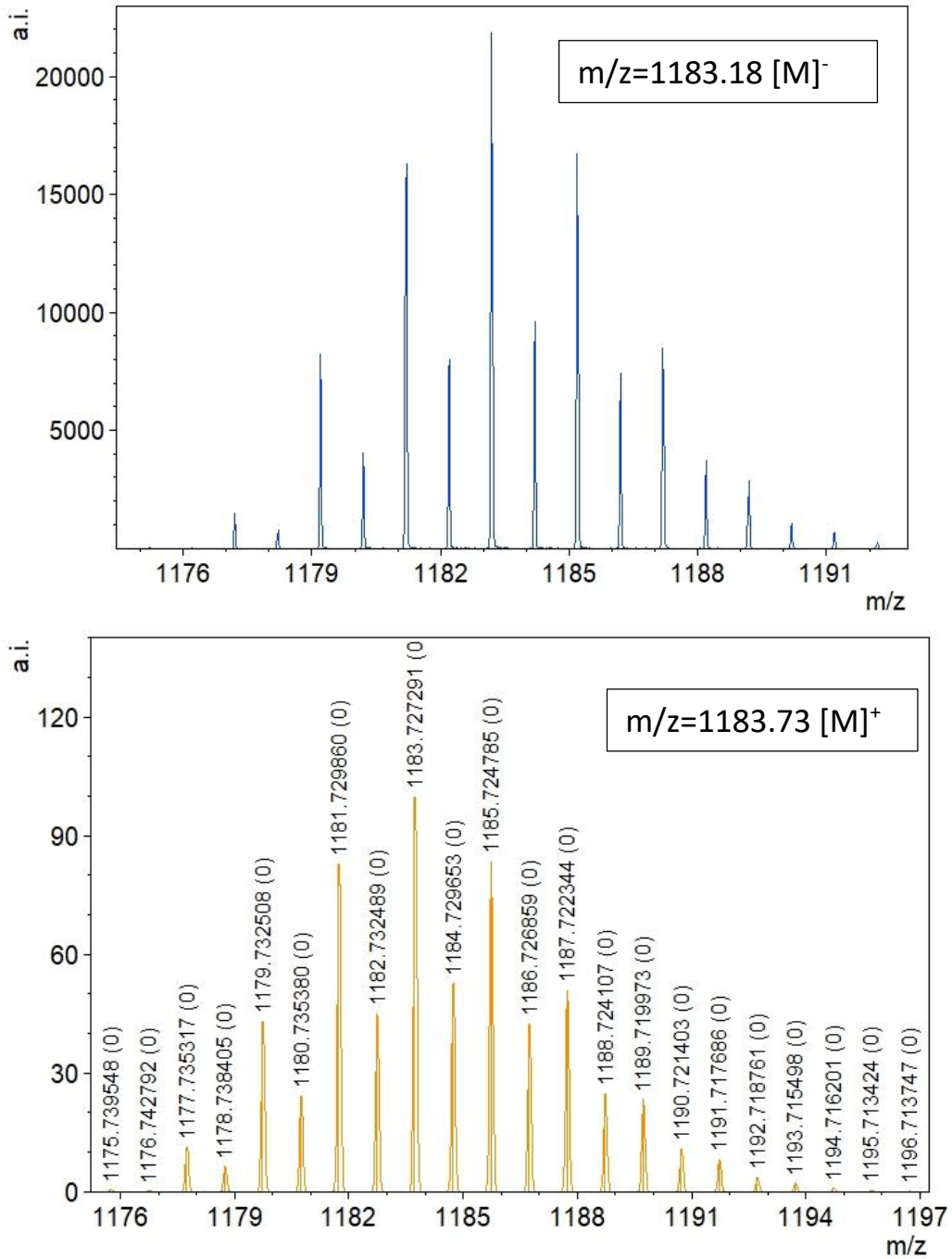

Figure S35: MALDI-ToF spectra of **3-Rad** experimental (top) and simulated (bottom), negative mode.

Cyclic voltammetry

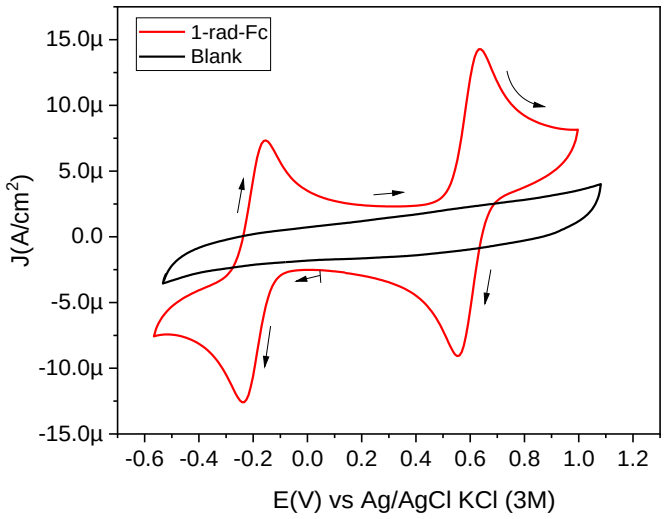

Figure S36: Cyclic voltammetry of **3-Rad** (0.35 mM) over a glassy carbon electrode using as electrolytic medium a 0.1M solution of $TBAPF_6$ in CH_2Cl_2, under argon atmosphere.

Square wave voltammetry

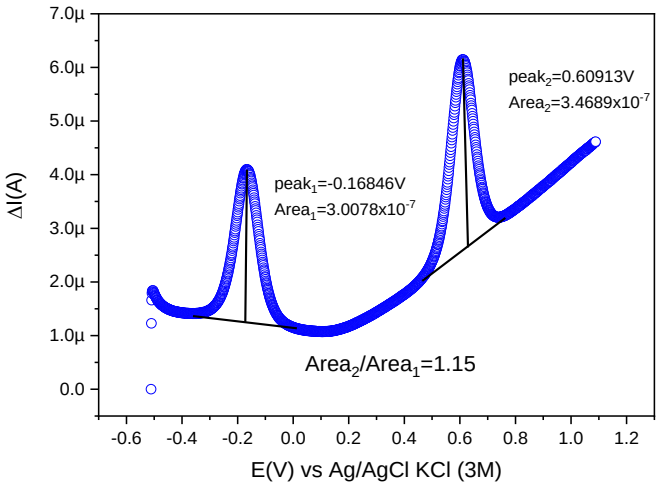

Figure S37: Square wave voltammetry of **3-Rad (**0.058 mM) over a glassy carbon electrode using as electrolytic medium a 0.1M solution of $TBAPF_6$ in CH_2Cl_2, under argon atmosphere. Step=1mV, $E_{modulation}$=20mV and Frequency=40Hz

rad-bisalkPTM-Fc$_2$ (4-Rad)

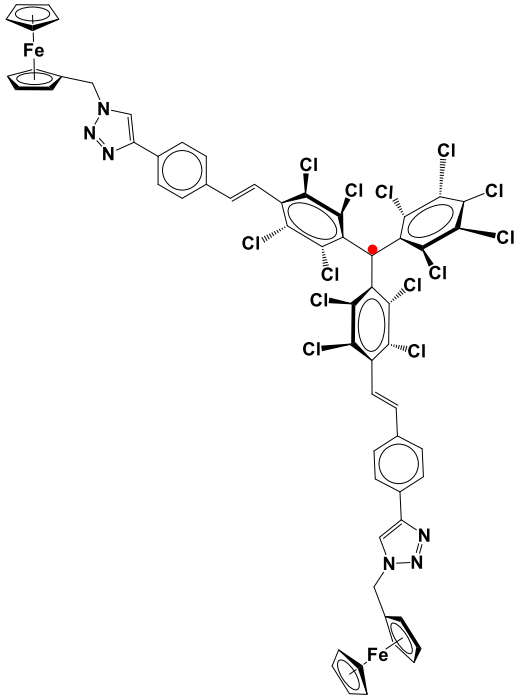

FT-IR

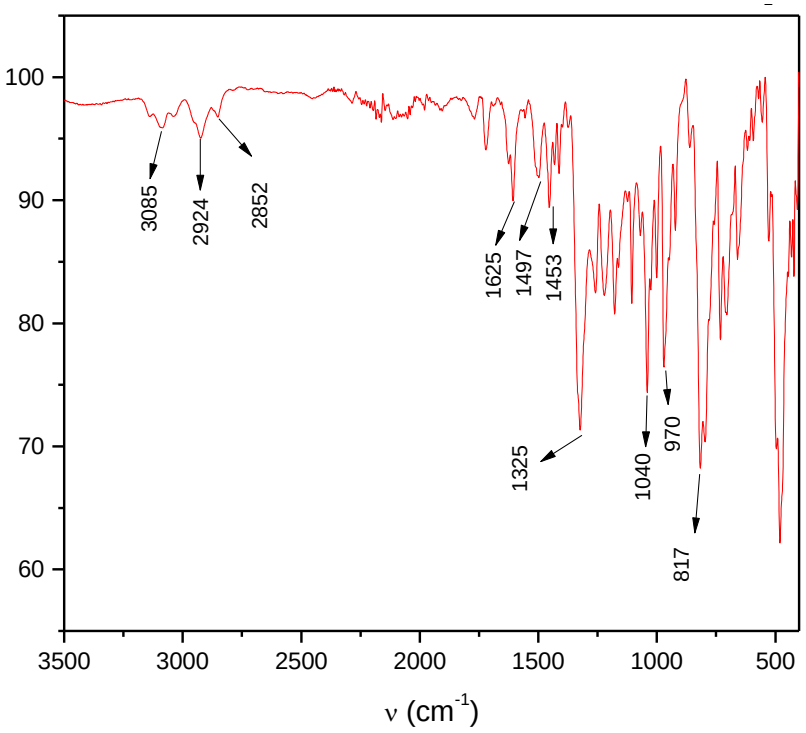

Figure S38: FT-IR spectrum of compound **4-Rad** in powder.

UV-Vis

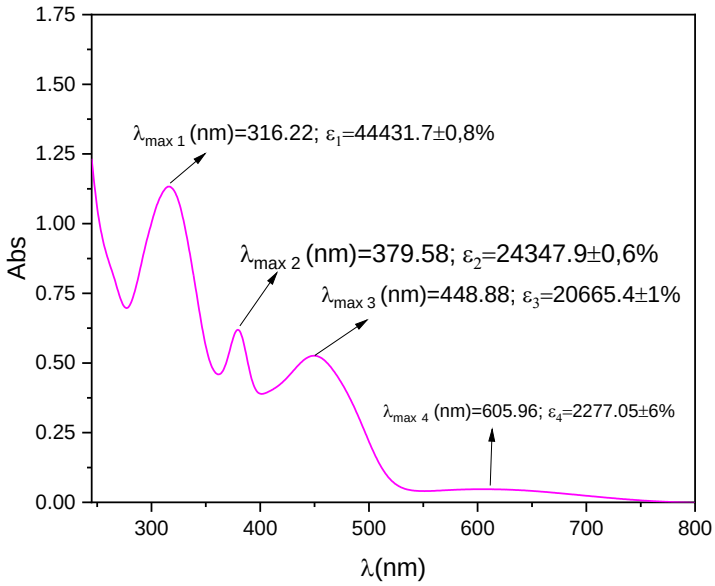

Figure S39: UV-Vis spectrum of **4-Rad** in CH_2Cl_2.
λ_{max} = maximum wavelength and ε= Molar absorptivity.

Electron paramagnetic resonance (EPR)

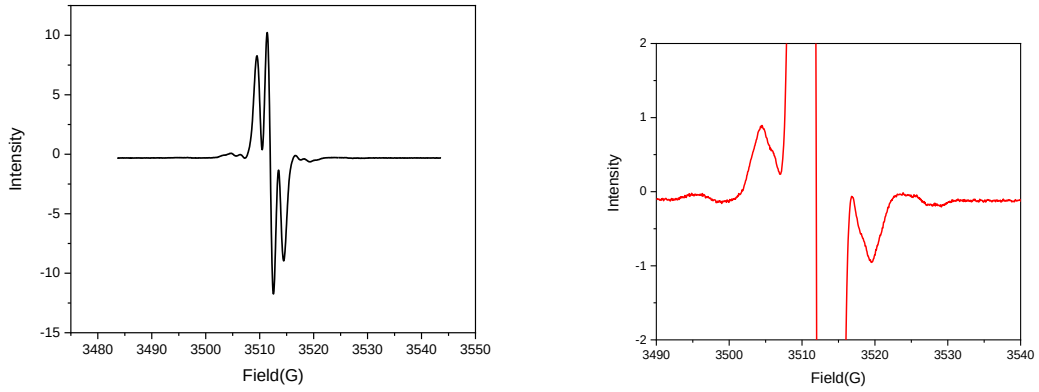

Figure S40: EPR spectra of **4-Rad** in dichloromethane at room temperature. The red spectrum (right) was recorded at higher power conditions.

MALDI-ToF

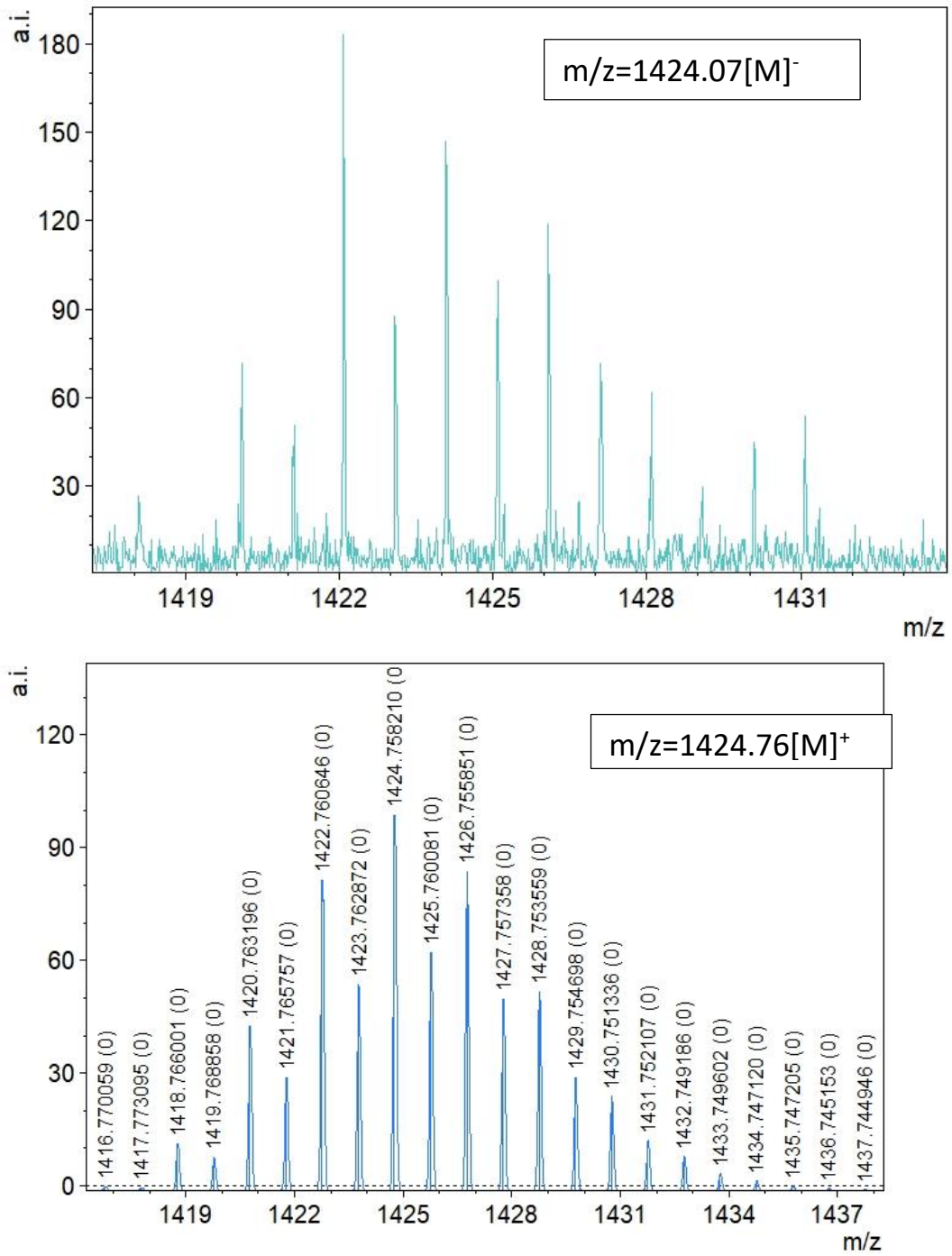

Figure S41: MALDI-ToF spectra of **4-Rad** experimental (top) and simulated (bottom), negative mode.

Cyclic voltammetry

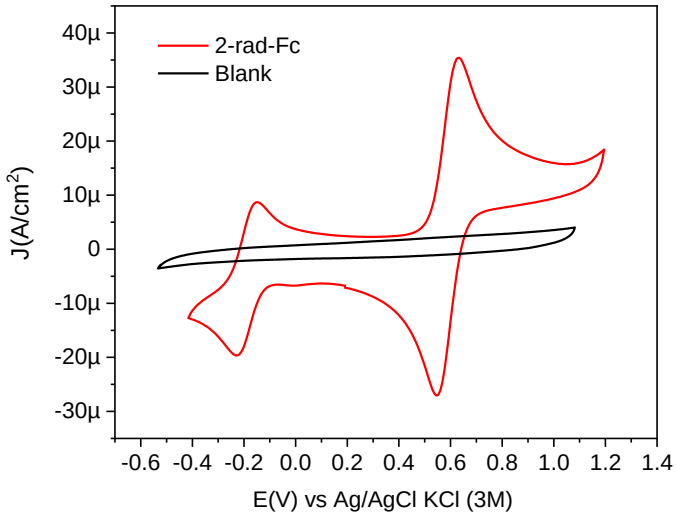

Figure S42: Cyclic Voltammetry of compound **4-Rad** (0.41 mM) over a glassy carbon electrode using as electrolytic medium a 0.1M solution of $TBAPF_6$ in CH_2Cl_2, under argon atmosphere.

Square wave voltammetry.

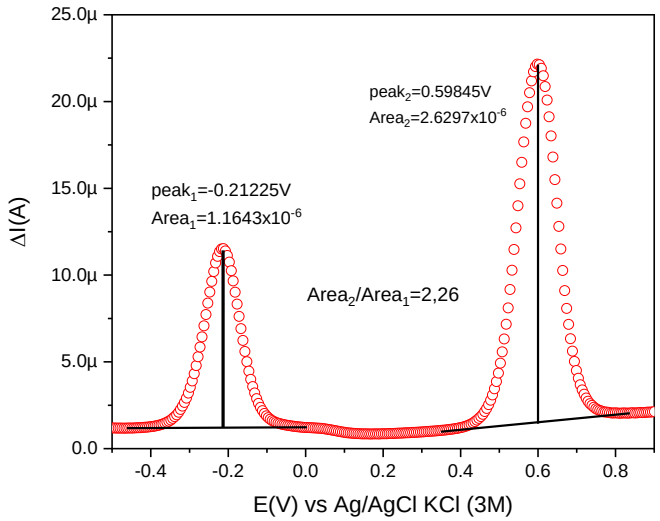

Figure S43: Square wave voltammetry of compound **4-Rad** (0.41 mM) over a glassy carbon electrode using as electrolytic medium a 0.1M solution of $TBAPF_6$ in CH_2Cl_2, under argon atmosphere. Step=5mV, $E_{modulation}$=20mV and Frequency=10Hz

References

(1) Stohr, J. *NEXAFS Spectroscopy*; Springer, 2003.

(2) Casu, M. B. Nanoscale Order and Structure in Organic Materials: Diindenoperylene on Gold as a Model System. *Cryst. Growth Des.* **2011**, *11*, 3629–3635.

(3) Casu, M. B.; Cosseddu, P.; Batchelor, D.; Bonfiglio, A.; Umbach, E. A High-Resolution near-Edge x-Ray Absorption Fine Structure Investigation of the Molecular Orientation in the Pentacene/Poly(3,4-Ethylenedioxythiophene): Poly(Styrenesulfonate) Pentacene/System. *J. Chem. Phys.* **2008**, *128*, 74702.

(4) Casas-Solvas, J. M.; Vargas-Berenguel, A.; Capitán-Vallvey, L. F.; Santoyo-González, F. Convenient Methods for the Synthesis of Ferrocene−Carbohydrate Conjugates. *Bioorg. Med. Chem. Lett* **1999**, *32*, 1–12.

(5) Park, K. M.; Thuo, M. M.; Whitesides, G. M.; Yoon, H. J.; Shapiro, N. D.; Soh, S. The Rate of Charge Tunneling through Self-Assembled Monolayers Is Insensitive to Many Functional Group Substitutions. *Angew. Chemie Int. Ed.* **2012**, *51*, 4658–4661.

(6) Wade, C. P.; Chidsey, C. E. D. Etch-Pit Initiation by Dissolved Oxygen on Terraces of H-Si(111). *Appl. Phys. Lett.* **1997**, *71*, 1679–1681.

(7) Alexander B. Sieval, Ralf Linke, Han Zuilhof, and E. J. R. S. High-Quality Alkyl Monolayers on Silicon Surfaces. *Adv. Mater.* **2000**, *12*, 1457–1460.

(8) Allen J. Bard Larry R. Faulkner. *Electrochemical Methods; Fundamentals and Applications*; John Wiley & Sons, Ltd, 2002.

(9) Eckermann, A. L.; Feld, D. J.; Shaw, J. A.; Meade, T. J. Electrochemistry of Redox-Active Self-Assembled Monolayers. *Coord. Chem. Rev.* **2010**, *254*, 1769–1802.

(10) Simeone, F. C.; Yoon, H. J.; Thuo, M. M.; Barber, J. R.; Smith, B.; Whitesides, G. M. Defining the Value of Injection Current and Effective Electrical Contact Area for EGaIn-Based Molecular Tunneling Junctions. *J. Am. Chem. Soc.* **2013**, *135*, 18131–18144.

(11) Reus, W. F.; Thuo, M. M.; Shapiro, N. D.; Nijhuis, C. A.; Whitesides, G. M. The SAM, Not the Electrodes, Dominates Charge Transport in Metal-Monolayer//Ga_2O_3/Gallium-Indium Eutectic Junctions. *ACS Nano* **2012**, *6*, 4806–4822.

(12) Savu, S. A.; Biswas, I.; Sorace, L.; Mannini, M.; Rovai, D.; Caneschi, A.; Chassé, T.; Casu, M. B. Nanoscale Assembly of Paramagnetic Organic

Radicals on Au(111) Single Crystals. *Chem. - A Eur. J.* **2013**, *19* (10), 3445–3450.

(13) Casu, M. B.; Schuster, B. E.; Biswas, I.; Raisch, C.; Marchetto, H.; Schmidt, T.; Chassé, T. Locally Resolved Core-Hole Screening, Molecular Orientation, and Morphology in Thin Films of Diindenoperylene Deposited on Au(111) Single Crystals. *Adv. Mater.* **2010**, *22*, 3740–3744.

(14) Savu, S. A.; Casu, M. B.; Schundelmeier, S.; Abb, S.; Tönshoff, C.; Bettinger, H. F.; Chassé, T. Nanoscale Assembly, Morphology and Screening Effects in Nanorods of Newly Synthesized Substituted Pentacenes. *RSC Adv.* **2012**, *2*, 5112–5118.

(15) Schöll, A.; Zou, Y.; Jung, M.; Schmidt, T.; Fink, R.; Umbach, E. Line Shapes and Satellites in High-Resolution x-Ray Photoelectron Spectra of Large π-Conjugated Organic Molecules. *J. Chem. Phys.* **2004**, *121*, 10260–10267.

(16) Sjögren, B.; Svensson, S.; Naves De Brito, A.; Correia, N.; Keane, M. P.; Enkvist, C.; Lunell, S. The C1s Core Shake-up Spectra of Alkene Molecules: An Experimental and Theoretical Study. *J. Chem. Phys.* **1992**, *96*, 6389–6398..

(17) Arantes, C.; Chernick, E. T.; Gruber, M.; Rocco, M. L. M.; Chassé, T.; Tykwinski, R. R.; Casu, M. B. Interplay between Solution Processing and Electronic Structure in Metal-Free Organic Magnets Based on a TEMPO Pentacene Derivative. *J. Phys. Chem. C* **2016**, *120*, 3289–3294.

(18) Kakavandi, R.; Savu, S. A.; Sorace, L.; Rovai, D.; Mannini, M.; Casu, M. B. Core-Hole Screening, Electronic Structure, and Paramagnetic Character in Thin Films of Organic Radicals Deposited on SiO_2/Si(111). *J. Phys. Chem. C* **2014**, *118*, 8044–8049.